JOURNAL OF GEOPHYSICAL RESEARCH, VOL. 112, F04008, doi:10.1029/2006JF000650, 2007

Turbulent flow and drag over fixed two- and three-dimensional dunes

Jeremy G. Venditti[1,2]

Received 1 August 2006; revised 5 May 2007; accepted 11 July 2007; published 16 November 2007.

[1] Detailed measurements of turbulent flow were obtained over a fixed flat bed, two-dimensional (2-D) dunes and four types of three-dimensional (3-D) dune morphologies including (1) full width saddles, (2) full width lobes, (3) sinuous crests, and (4) irregular shaped crests. The time-averaged turbulence structure over the fixed flat bed was dynamically similar to flow over a flat bed with active sediment transport. The flow field over 2-D dunes conforms with previous observations of flow over mobile and fixed bed forms. Bed form three dimensionality significantly altered the flow field observed over the 2-D dunes. Lobe-shaped dune crest lines, curved crests with topographic highs that bowed downstream, enhanced the level of turbulence producing a better defined wake structure and more vigorous mixing in the separation cell than observed over 2-D dunes. Saddle-shaped dune crest lines, curved crests with topographic highs that bowed upstream, diminished the level of turbulence suppressing a well-defined wake structure and mixing in the flow separation cell. Flow over sinuous-crested bed forms with lobes and saddles was dynamically similar to flow over full width bed forms. Development of in-line paired saddles and lobes in the downstream direction appears to be controlled by near-bed velocity gradients, which were larger over saddles and smaller over lobes. These gradients control local boundary shear stress patterns that should promote scour and high transport rates over saddles and deposition on lobes. Two-dimensional and 3-D bed forms with the same height and length offered different levels of flow resistance. The flow observations support the idea that saddles decrease flow resistance and lobes increase flow resistance relative to a 2-D dune. Bed form crests composed of irregularly spaced lobes and saddles suppressed turbulent flow structure development and reduced drag by 20% below levels for 2-D or sinuous crested dunes. The results suggest that bed form crest shape needs to be accounted for in flow resistance calculations and that a single drag coefficient is inadequate where the bed can evolve through 2-D, 3-D, and irregular 3-D bed form states.

Citation: Venditti, J. G. (2007), Turbulent flow and drag over fixed two- and three-dimensional dunes, *J. Geophys. Res.*, *112*, F04008, doi:10.1029/2006JF000650.

1. Introduction

[2] Sand-bedded alluvial channels regulate flow resistance through the development of bed forms of various scales and forms (i.e., ripples, dunes, and bars). This mechanism promotes stability in channels that contain flows that can readily erode the bed and banks at modest discharges. When not parameterized directly from flow measurements, flow resistance in sand bedded channels is typically parameterized in terms of bed form scales (height H, length, L). As such, bed form growth and diminution are considered the primary way flow resistance is regulated. Yet, there is evidence that morphologic transitions, independent of bed form size are ubiquitous during the development of bed forms and that bed form morphology can strongly modulate flow resistance.

[3] It has been demonstrated that there is an inevitable transition that occurs between 2-D and 3-D bed forms if a constant flow is maintained for a sufficient period of time and the cross-stream flow is not suppressed (see work on the 2-D to 3-D transition of ripple bed geometries by J. H. Baas and collaborators [cf. *Baas et al.*, 1993; *Baas*, 1994, 1999] and of dune bed geometries by *Venditti et al.* [2005a]). These 3-D morphologies *are* the equilibrium bed state that varies with time but is pattern stable. *Best* [2005a] in a review of the fluid dynamics over dunes noted that there is an urgent need to explore the linkage between 3-D bed form morphology, turbulence, and boundary shear stress in order to understand bed form mechanics and flow resistance properties in open channel flow. Yet, it remains unclear what effects the transition from 2-D to 3-D bed morphology has on the turbulent flow field and, fundamentally, on resistance to flow in river channels.

[1]Department of Earth and Planetary Sciences, University of California, Berkeley, California, USA.
[2]Now at Department of Geography, Simon Fraser University, Burnaby, British Columbia, Canada.

0148-0227/07/2006JF000650$09.00

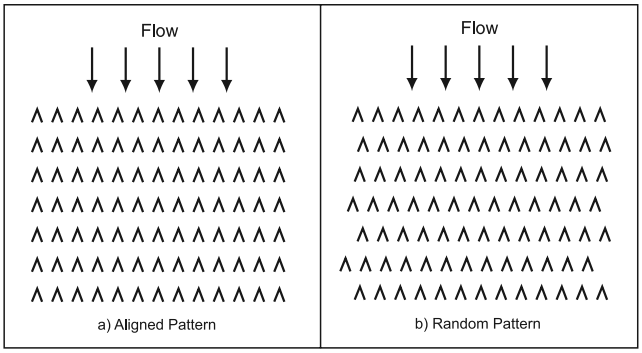

Figure 1. Plan view of (a) strictly two-dimensional aligned pattern and (b) out-of-phase random pattern of riblets examined by *Sirovich and Karlsson* [1997].

[4] A number of studies over the past 15 years have identified the main characteristics of the flow field over 2-D dunes [cf. *Wiberg and Nelson*, 1992; *Lyn*, 1993; *Nelson et al.*, 1993; *McLean et al.*, 1994; *Bennett and Best*, 1995; *Venditti and Bennett*, 2000], which has led to increasingly realistic simulations of the turbulent flow field [*Schmeeckle et al.*, 1999; *Shimizu et al.*, 1999, 2001; *Zedler and Street*, 2001]. Summary sketches of the flow structure over 2-D fixed bed forms can be found elsewhere [*McLean*, 1990; *Venditti and Bauer*, 2005; *Best*, 2005a], but the main characteristics are (1) convergent, accelerating flow over the dune stoss, (2) flow separation at the dune crest, (3) flow reattachment at $\sim 4-6 \times$ bed form height [*Engel*, 1981; *Bennett and Best*, 1995; *Venditti and Bennett*, 2000], (4) a turbulent wake and shear layer originating at the crest, extending and expanding downstream, (5) an internal boundary layer (IBL) that grows from the reattachment point downstream beneath the wake toward the crest, and (6) an outer, overlying wake region [see *Nelson et al.*, 1993; *McLean et al.*, 1994; *Bennett and Best*, 1995; *Venditti and Bennett*, 2000]. Three-dimensional rollers, kolks, and internal boils occur along the shear layer, dominating the macroturbulent flow structure [*Nezu and Nakagawa*, 1993]. See *Best* [2005a, 2005b] for detailed reviews of the spatial and temporal flow structure over dunes.

[5] Far less work has focused on the turbulent flow field over 3-D bed forms. The seminal work of *Allen* [1968] is the most extensive study of near-bed flow over 3-D bed forms. He illustrated the complexity of flow over 3-D morphologies and the influence that the near-bed flow, particularly the flow separation pattern, has on sand movement. Yet, the characteristics of the flow field above the near-bed area and the effect of 3-D morphology on flow resistance were not investigated by *Allen* [1968]. Recently, considerable progress was made by *Maddux et al.* [2003a, 2003b], who examined the whole flow field over straight-troughed dunes with a cross-stream variation in dune height (referred to herein as quasi-3-D forms). By maintaining a constant lee slope, the fixed dune crests curved across the channel forming saddles at high points and lobes at low points. The resistance of the quasi-3-D forms was much larger than over 2-D features, but the level of turbulence was much lower, owing to form-induced stresses associated with secondary flow circulations. A similar increase in shear stress with a decline in the level of turbulence was observed by *Schindler and Robert* [2005] as 2-D dunes became 3-D in active transport experiments.

[6] There is also reason to suspect that roughness element configuration, in the absence of secondary circulation, can cause reductions in the level of turbulence. *Sirovich and Karlsson* [1997] studied flow over "riblets" in an effort to determine what sort of patterns would effectively reduce drag on airplane surfaces. They demonstrated that a strictly 2-D aligned pattern (Figure 1a) produced a larger drag than a smooth surface while an out-of-phase random pattern (Figure 1b) produced a lower drag than a smooth surface. This occurred because random orientations of riblets effectively modulate the burst-sweep cycle, reducing boundary shear stress. *Sirovich and Karlsson* [1997] found that hydraulic drag was reduced by up to 20% by changing the arrangement of perturbations. The transition between 2-D and 3-D bed forms is analogous to a change from an aligned to a random pattern of roughness elements, with the complication that the 3-D bed forms induce secondary flow circulations. Thus it is of interest to expand upon the work of *Maddux et al.* [2003a, 2003b] by further exploring how different patterns of 3-D bed forms affect the turbulent flow field and flow resistance.

[7] Here, I examine flow over various bed form morphologies commonly observed in dune fields in natural rivers [cf. *Kostaschuk and MacDonald*, 1988; *Parsons et al.*, 2005] and, in particular, features observed in laboratory experiments reported by *Venditti et al.* [2005a]. Examination of flow over these types of bed forms in a mobile bed scenario remains a significant challenge because, in addition to migrating downstream, these bed forms are constantly adjusting their heights and lengths in response to localized changes in sediment transport. Thus experiments were designed to look at flow over fixed, fully 3-D bed form morphologies with the following crest shapes: (1) straight-crested 2-D, (2) full width saddle (crest line bowed upstream), (3) full width lobe (crest line bowed downstream), (4) sinuous crest, and (5) irregular staggered crest. Use of irregular crest shape is motivated by suggestions that roughness elements arranged in irregular patterns can significantly reduce drag [cf. *Sirovich and Karlsson*, 1997] in turbulent flows.

[8] The observations are used to examine the effects of bed form three dimensionality on momentum transfer, mixing, and energy exchanges from the mean flow to turbulence. The near-bed flow patterns are used to explore the mechanism behind the development of in-line paired lobes and saddles. Finally, the impact of the crest line three dimensionality on total flow resistance is discussed in the context of the ideas of *Sirovich and Karlsson* [1997] and *Maddux et al.* [2003a].

2. Experimental Procedure

[9] The experiments were conducted in the Civil Engineering Hydraulics Laboratory at the University of British Columbia using a tilting flume channel, 17 m long, 0.515 m wide and 1 m deep. The head box exit was fitted with a 25.4 mm honeycomb that was 0.3 m long, and a water surface float, to ensure quasi-uniform flow out of the head box and eliminate water surface waves. An adjustable sluice

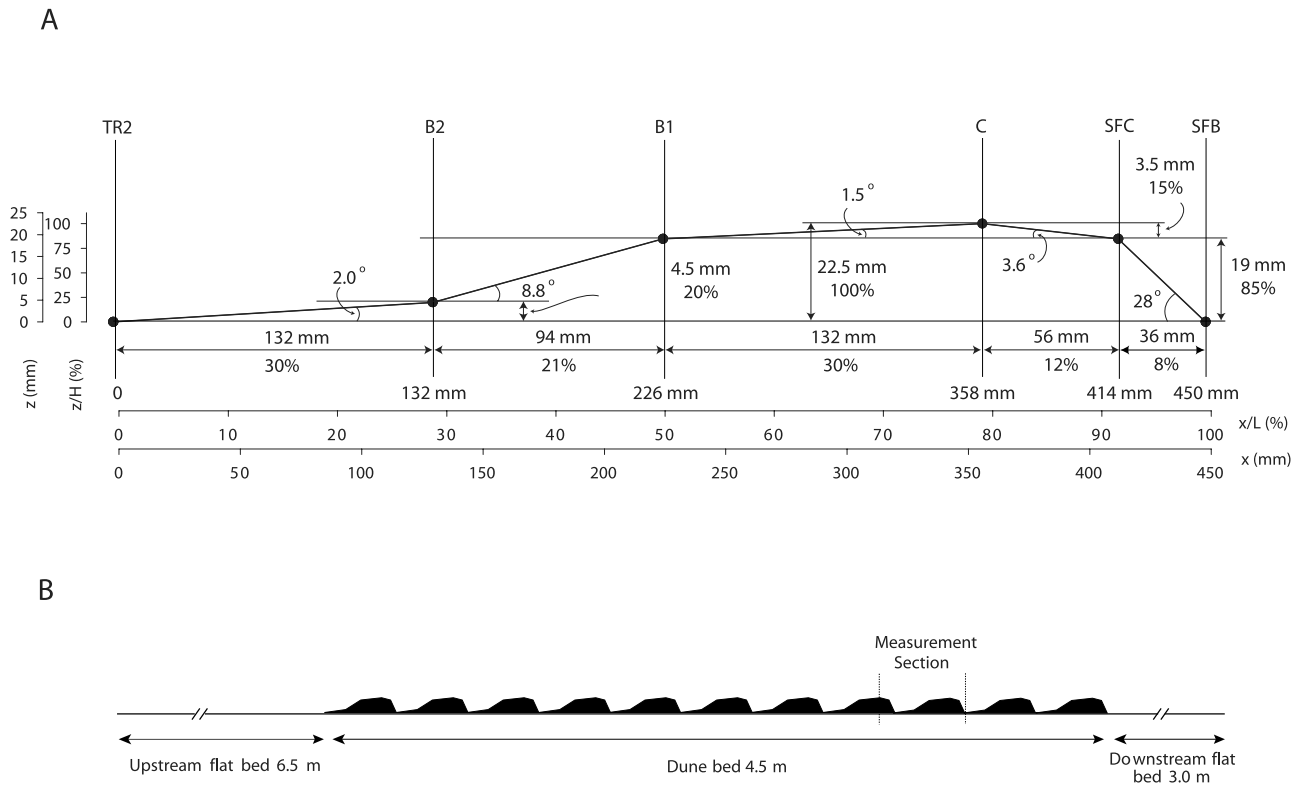

Figure 2. (a) Dune morphology determined from active transport experiments. A number of slope breaks were consistently observed during the NSL experiments and included the slip face base (SFB), slip face crest (SFC) dune crest (C), stoss slope breaks (B1 and B2) and dune trough (upstream is Tr2 and downstream is Tr). Measurements of these features from flow B were nondimensionalized by the associated bed form height H and length L to form a dimensionless prototype bed form shape (see *Venditti* [2003] for further details). Vertical height above the dune trough z and distance along the dune x were obtained by multiplying the dimensionless heights and lengths of features by the desired H (22.5 mm) and L (0.45 m). (b) Location of fixed bed forms in channel.

gate at the downstream end of the flume controlled the width of exiting flow and, ultimately, flow depth. Water was recirculated through an underground sump tank. Flow rate was controlled by a screw valve installed on the inflow pipe to the head box reservoir. An acoustic pipe flowmeter, mounted upstream of the control valve, ensured that discharge was maintained to within $\pm 3.3 \times 10^{-4}$ m^3 s^{-1}. Channel slope was adjusted using a mechanical jack mechanism that allowed submillimeter (±0.25 mm) vertical adjustments of the flume tail. Thus flume slope adjustment was accurate to $\pm 2.8 \times 10^{-5}$.

2.1. Fixed Bed Form Design

[10] The bed form shape template was based on observations from "active transport" experiments conducted in a 1 m wide flume using 0.5 mm sand at the National Sedimentation Laboratory, U.S. Dept. of Agriculture in Oxford Mississippi (henceforth referred to as NSL experiments). The experiments are described in detail by *Venditti et al.* [2005a, 2005b, 2005c]. Bed form profiles, drawn from echo soundings during one of the active transport experiments (flow B of *Venditti et al.* [2005a]), were normalized by the bed form height and length to produce a nondimensional model bed form (Figure 2). Dimensions were then imposed on the model shape by selecting a bed form length and maintaining the average observed aspect ratio H/L to set height.

[11] There was a pronounced transition between 2-D and 3-D bed forms during the first hour of the NSL experiments when the bed forms were growing [*Venditti et al.*, 2005a]. At the transition, $H \approx 10$ to 15 mm and $L \approx 0.2$ to 0.3 m and it would have been desirable to have used these bed forms dimensions in the experiments described herein. However, the bed forms would have been too small to take usefully resolved flow measurements with the available instrumentation (an acoustic Doppler velocimeter or ADV). As a compromise, $L = 0.45$ m was selected as a desired length. Average aspect ratio for the flow conditions in Table 1 was $H/L \approx 0.05$, giving $H = 22.5$ mm. The resulting morphology appears in Figure 2a.

[12] Bed forms were constructed from 4.88 m × 38 mm × 89 mm pressure treated wooden planks (finished 16 ft, 2 × 4, dimensional lumber). The bed form shape was carved into each 2 × 4 plank eleven times and the boards were bolted together to form bed forms that spanned the flume channel (Figure 3). The consistency of the carved bed form heights was held to within ±1 mm.

Table 1. Summary of Flow Parameters[a]

Flow Parameter	Flow B	Flat	2-D	FWL	FWS	IRR	Sinuous (SNL/SNS)	SSS
NDS	-	-	1.0	1.43	1.43	2.31	1.33	1.33
Q,[b] m^3 s^{-1}	0.0723	0.0376	0.0376	0.0376	0.0376	0.0376	0.0376	0.0376
d_{min}, m	-	-	0.139	0.141	0.141	0.146	0.144	0.145
d_{max}, m	-	-	0.164	0.163	0.162	0.170	0.166	0.168
$\overline{d}$, m	0.152	0.152	0.151	0.152	0.153	0.157	0.155	0.156
$\overline{U}$, m s^{-1}	0.477	0.479	0.485	0.480	0.476	0.465	0.471	0.467
Fr	0.39	0.39	0.40	0.39	0.39	0.38	0.38	0.38
Re	72300	73010	73010	73010	73010	73010	73010	73010
$S \times 10^{-3}$	1.06	0.767	1.23	1.40	1.68	0.957	1.29	1.18
τ, Pa	1.54	1.04	1.66	1.89	2.29	1.33	1.77	1.63
$u*$, m s^{-1}	0.041	0.032	0.041	0.044	0.048	0.036	0.042	0.040
C_d	0.0069	0.0045	0.0070	0.0082	0.0101	0.0061	0.0080	0.0075

[a]Shear stresses are corrected for sidewall effects using the relation supplied by *Williams* [1970].
[b]There is a slight difference (<1%) in the unit discharges between the two experiments because initial scaling of the fixed bed flow was calculated using a channel width of 0.520 m rather than the actual channel width of 0.515 m. $\overline{U} = Q/(\overline{d} \cdot y_w)$, $Fr = \overline{U}/\sqrt{g\overline{d}}$, $Re = \overline{U}\,\overline{d}/\nu$, $\tau = \rho_w g \overline{d} S$, $u* = \sqrt{\tau/\rho_w}$, $C_d = (u*/\overline{U})^2$.

[13] By staggering the alignment of the boards, various dune crest line configurations could be generated (Figure 3). A straight-crested 2-D dune was created by lining up the crests carved in the wooden planks. Conventional 3-D dunes were designed with crest lines that bowed over the whole flume width downstream (full width lobes; FWL) and upstream (full width saddles; FWS). Sinuous-crested bed forms were composed of two lobes (SNL), one saddle (SNS) in the center of the flume and two half saddles at the sidewalls with approximately the same crest line sinuosity as the full width bed forms (Table 1). During a separate experimental run, the slip face of the sinuous bed form crest line was smoothed across the entire flume width with wood filler to remove the jagged edge, producing a new bed morphology, a sinuous and smooth saddle (SSS). This provided an opportunity to examine the effect of the jagged dune face on shear stress estimates. In order to determine applicability of the ideas of *Sirovich and Karlsson* [1997] to dune bed forms, an irregular crest orientation (IRR) was produced by staggering the boards in an apparent random fashion. This was the most common crest line observed in the NSL experiments [see *Venditti et al.*, 2005a].

[14] Model bed form crest line sinuosity was based on observations from the NSL experiments. *Venditti et al.* [2005a] examined the variation in crest line sinuosity (referred to as nondimensional span, NDS = L_c/L_y, where L_c is the crest line length and L_y is the linear distance between the crest endpoints, herein where the crests intersect the flume walls) as bed forms grew and changed from 2-D to 3-D. They found NDS, averaged along stream over 1.2 channel widths, increased from ~1.0 for 2-D dunes to a value of ~1.4 when the transition was complete and that NDS typically varied between 1.2 and 2.5 when the dunes were 3-D. In light of this, full width and sinuous bed forms were designed with NDS = 1.4 and 1.3, respectively. The more complicated IRR crest line configuration had NDS ≈ 2.4.

[15] Upstream and downstream of the dune configured bed, a flat bed section was installed at the level of the first dune trough. The flat bed extended ~6.5 m downstream from the head box and ~3 m downstream of the dune field (Figure 2b). The flat and dune field portions of the bed were painted with contact cement to which a layer of 0.5 mm sand was adhered to simulate skin roughness. Differences between the slope of these bed inserts and the channel slope were checked externally using a theodolite and aluminum meter stick as well as point gauges. In some cases, the flume

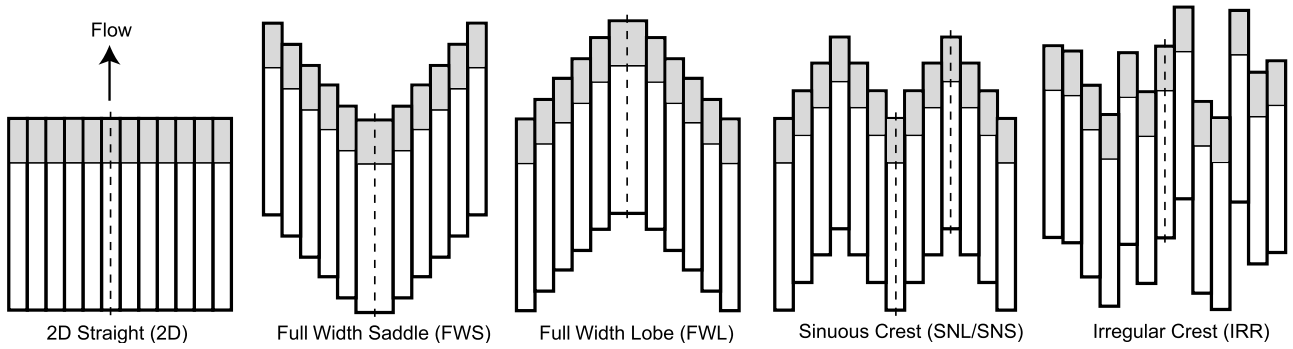

Figure 3. Dune morphologies tested. Grey areas are in the lee of the dune crest on each plank. Lines down the center (and along the right lobe of the sinuous crest) indicate where the velocity profiles were taken.

slope differed slightly from the dune bed insert slope. If the difference exceeded $\pm 8.3 \times 10^{-5}$, the slope reported in Table 1 was corrected accordingly.

2.2. Flow Conditions

[16] The flow conditions established during flow B in the NSL experiments were reproduced over the fixed bed forms. The experiments were run at the same discharge per unit width (0.0723 $m^2\ s^{-1}$). In order to compare flow over the fixed flat bed and the mobile flat bed of the NSL experiments, an attempt was made to match the depth d, bulk mean velocity $\overline{U}$, and water surface slope S. This was done by adjusting the sluice gate and the flume tilt to provide constant depths over the upstream flat portion of the bed. The slope necessary to achieve the NSL experiment d and $\overline{U}$ over the fixed flat bed corresponded to a lower model S (Table 1), which translates to a shear stress ($\tau = \rho_w g \overline{d} S$) that was ~68% of τ for the mobile bed NSL experiment. The difference likely reflects a minor increase in form roughness as the mobile bed organized nascent bed features and the influence of the transport layer in the NSL experiments [cf. *Best et al.*, 1997].

[17] Over the 2-D dune bed, the sluice gate opening and S were adjusted so that d over the crests was similar to d over the flat bed. Quasi-equilibrium flow was achieved by adjusting the slope to obtain the same depth (±0.3 mm) over five successive bed form crests. Over subsequently tested dune configurations, the sluice gate opening was maintained so that only the flume tilt was adjusted to attain quasi-equilibrium flow. As such, d and $\overline{U}$ are a function of flume tilt (ultimately S) and crest line configuration. The standard error of measured flow depths over the dune insert crests was <0.2% over each bed.

[18] Table 1 summarizes the bulk hydraulic conditions for each crest configuration. Only one set of hydraulic conditions is presented for the sinuous crests (SNS and SNL). The mean flow depth $\overline{d}$ was calculated as

$$\overline{d} = d_{\min} + H(1-\beta) + \frac{z_{WS-\max} - z_{WS-\min}}{2}, \qquad (1)$$

where $d_{\min}$ is the minimum depth (over the crest), β is the bed form shape factor ($\beta = A/HL = 0.56$; A is the cross-sectional area of the bed form [*Venditti et al.*, 2005c]), $z_{WS-\max}$ is the maximum water surface over the dune length, and $z_{WS-\min}$ is the minimum water surface over the dune length.

2.3. Potential Errors in Flow Depth, Velocity, and Slope

[19] The bulk hydraulic quantities for the different bed configurations are compared, and in some cases the errors associated with these quantities are as large as the differences between different beds therefore necessitating a clear statement of potential error. Flow depths, water surface elevation, and bed form height were measured with a point gauge with 0.3 mm increment. Thus the error associated with the flow depth, propagated through equation (1), is <1 mm. The error in the bulk mean velocity, derived from the uncertainty in Q and $\overline{d}$ is quite substantial: ±4.5 mm s^{-1}. Potential errors in the flume slope include error associated with the slope adjustment reading ($\pm 2.8 \times 10^{-5}$) and the potential difference between the flume slope and the bed form insert ($\pm 8.3 \times 10^{-5}$). When these uncertainties in slope and depth are propagated through the total bulk shear stress calculation ($\tau = \rho_w g \overline{d} S$), the resultant error in the total boundary shear stress is on the order of ±0.15 Pa.

2.4. Velocity Measurements and Analysis

[20] Velocity measurements were obtained using an ADV that measured three-component flow velocities (streamwise, u; cross-stream, v; and vertical, w) at 50 Hz. The ADV has a manufacturer reported precision of ±0.1 mm s^{-1} and the sampling volume is located ~50 mm from the probe [*Sontek*, 1997]. ADV signals are affected by Doppler noise, or white noise, associated with the measurement process [*Lohrmann et al.*, 1994]. The presence of this noise at high frequencies may create an aliasing effect where energy at frequencies greater than the Nyquist frequency (herein f_n = 25 Hz) are "folded" into frequencies lower than f_n. Thus the maximum resolvable frequency is 25 Hz. To remove possible aliasing effects, a Gaussian low-pass filter with a half power frequency of 25 Hz was applied to the velocity time series [*Biron et al.*, 1995; *Lane et al.*, 1998].

[21] The ADV software provides signal quality information in the form of a correlation coefficient r_{ADV}. The manufacturer suggests that when r_{ADV} does not exceed 0.7, the instantaneous velocity measurement is dominated by acoustic noise and, as a rule of thumb, that these measurements should be discarded [*Sontek*, 1997]. It has been recognized that signal quality is reduced in highly turbulent regions of flow due to shear in the sampling volume and that the threshold r_{ADV} may be <0.7 (see sensitivity analysis of *Martin* [2002]). Indeed, the measurements presented herein indicated that low r_{ADV} values occurred in highly turbulent regions of flow; near the bed, along the lee slope and in the separation zone. Careful examination of the time series revealed that poor correlations were not associated with particular turbulent motions.

[22] In recognition of this, a filter was designed to remove instantaneous velocity measurements in the time series when r_{ADV} did not exceed 0.7. At-a-point, time-averaged measurements were discarded from the data set when r_{ADV} did not exceed 0.7 for >70% of the record. However, when the measurement was near the bed, along the lee slope of the dunes or in the separation zone, at-a-point, time-averaged measurements were accepted when r_{ADV} exceeded 0.7 for >40% of the record. At a sampling rate of 50 Hz, a record in which only 40% is retained is still sampled at a nominal rate of 20 Hz.

[23] A test section was defined over the eighth dune, 9.5–10.0 m downstream of the flume entrance (Figure 2b). Over each bed configuration, a total of 35–37 profiles of velocity were taken along the flume centerline and spaced at 0.014–0.018 m apart. Each profile consisted of 10–15 vertical measurement locations sampled for 90 s. Over the sinuous crest line, the centerline profiles were over a saddle (SNS). Another set of profiles was taken nearer to the sidewall over a lobe (SNL) (Figure 3). In addition to the profiles over the dunes, 6 profiles were taken over the flat bed at 0.10 m intervals between 5.0 and 5.5 m when the 2-D dunes were installed further down the channel.

[24] For most measurements, the ADV probe head was oriented toward the bed at 0°. The lowest point in each

velocity profile was at a height of ~5 mm above the bed and the highest point was at ~0.08–0.11 m, depending on the position over the dune. Poor data quality caused by acoustic feedback was observed at several heights above the bed and this is a common feature of ADV measurements [see *Lane et al.*, 1998]. In order to obtain data at these heights, the ADV probe head was rotated 45° in the cross-stream plane, which eliminated the feedback. To augment the velocity profiles, the ADV probe head was also rotated 90° in the cross-stream plane to obtain a measurement that was typically 0.11–0.12 m above the dune crests. In the 45° and 90° orientations, the position of the sensor was adjusted such that the sampling volume was always in same plane as measurements taken with a 0° probe orientation.

[25] Data collected when the probe head was at 45° and 90° needed to be rotated into the vertical plane. The streamwise velocity has the same magnitude and direction, regardless of whether the probe was in the 0°, 45°, or 90° positions. Thus the data need to be rotated only in the *v*-*w* plane. The *v* and *w* velocity components were rotated according to the following convention:

$$\begin{aligned} v_{rp} &= v_m \cos\varphi + w_m \sin\varphi \\ w_{rp} &= -v_m \sin\varphi + w_m \cos\varphi, \end{aligned} \tag{2}$$

where subscripts *m* and *r* refer to the measured and rotated velocity frames, respectively, and φ is the angle of the probe head (0°, 45° or 90°). The subscript *p* indicates the rotation is necessary for realignment when the probe is in the 45° or 90° position.

[26] Care was taken in orienting the probe head so that it was aligned with the maximum streamwise velocity in the 0°, 45°, or 90° positions. However, small misalignments were still common, which presented the possibility of having slightly different planes of reference for the measurements in different configurations. This is a potentially serious problem when different probe head alignments are used. Therefore rotations are necessary in the *u*-*v* and *u*-*w* plane. A *u* and *v* rotation follows the convention

$$\begin{aligned} u_{ra} &= u_m \cos\gamma + v_{rp} \sin\gamma \\ v_{ra} &= -u_m \sin\gamma + v_{rp} \cos\gamma, \end{aligned} \tag{3}$$

where γ is a misalignment angle in the *u*-*v* plane and the subscript *a* distinguishes this rotation from the realignment necessary when the probe is in the 45° or 90° position. A *u* and *w* rotation follows the convention

$$\begin{aligned} u_{ra2} &= u_{ra} \cos\phi + w_{rp} \sin\phi \\ w_{ra} &= -u_{ra} \sin\phi + w_{rp} \cos\phi, \end{aligned} \tag{4}$$

where ϕ is a misalignment angle in the *u*-*w* plane and the subscript 2 indicates that this is the second rotation of the *u* component.

[27] In order to estimate the rotation angles γ and ϕ, calibration files were taken each time the probe was readjusted at 0.06 and 0.09 m above the flat bed portion of the flume at 5.0 m from the head box, where the *v* and *w* components of velocity could be expected to average to zero. By assuming the mean v_{ra} velocity is zero, equation (3) can be rearranged such that

$$\gamma = \tan^{-1} \frac{V_{rp}}{U_m} \tag{5}$$

(uppercase *u*, *v* and *w* represent mean at-a-point velocities). In order to estimate ϕ, the data need to be rotated by applying equation (3). Then, assuming mean w_{ra} velocity is zero, equation (4) can be rearranged such that

$$\phi = \tan^{-1} \frac{W_{rp}}{U_{ra}}. \tag{6}$$

Values of γ and ϕ varied between −4° and 3° but were typically smaller. Data collected over the dunes are then rotated by γ and ϕ using equations (3) and (4), placing the entire data set in the same plane of reference. By approaching the rotations in this manner, deviations in the mean vertical and cross-stream velocities over the dunes are accepted as real.

3. Previous Work on Structure of Flow Over Flat and 2-D Dune Beds

[28] In the work presented here, the flow fields over the various bed configurations are examined empirically via several simple turbulence and velocity relations, including the mean streamwise and vertical velocities, turbulence intensity, streamwise and vertical Reynolds stress, and the turbulent kinetic energy. Before presenting the results, it is of interest to first review the characteristics of flow fields over flat and 2-D dune beds, as elucidated through previous examinations of these simple velocity and turbulence relations. The descriptions of flow over 2-D dunes are based on work by *Nelson et al.* [1993], *McLean et al.* [1994], *Bennett and Best* [1995] and *Venditti and Bennett* [2000], unless otherwise indicated. The focus of each of these studies is different, but descriptions of the flow field are consistent.

[29] Time-averaged streamwise *U* and vertical *W* flow velocities are defined as

$$U = \frac{1}{n}\sum_{i=1}^{n} u_i \quad \text{and} \quad W = \frac{1}{n}\sum_{i=1}^{n} w_i, \tag{7}$$

where u_i and w_i are instantaneous velocities and *n* is the total number of measurements. In uniform flow over a flat bed, *U* and *W* do not vary along flow. Flow over a 2-D dune is highly nonuniform, accelerating over the dune stoss slope due to convergence, and decelerating over the dune trough due to expansion. The vertical velocity responds with flow directed toward the bed downstream of the lee slope and toward the water surface over the stoss slope.

[30] Turbulence intensity is defined as

$$I_u = \frac{U_{rms}}{u*}, \tag{8}$$

where U_{rms} is the streamwise root-mean-square velocity

$$U_{rms} = \left[\frac{1}{n}\sum_{i=1}^{n} (u_i - U)^2\right]^{0.5} \tag{9}$$

and u_* is the shear velocity calculated from the depth-slope product. Over a flat bed, *Nezu and Nakagawa* [1993] indicate I_u should increases exponentially toward the bed [cf. *Venditti et al.*, 2005b]. Previous research suggests that, over 2-D dunes, maximum I_u values occur just downstream of reattachment and local highs occur within and just downstream of the flow separation cell. Elevated U_{rms} values typically occur in the highly turbulent wake region.

[31] The Reynolds shear stress τ_{uw} is determined using

$$\overline{u'w'} = \frac{1}{n}\sum_{i=1}^{n}(u_i - U)(w_i - W) \tag{10}$$

$$\tau_{uw} = -\rho_w \overline{u'w'}. \tag{11}$$

For steady uniform flow over a flat sand bed, τ_{uw} should increase linearly from near zero at the water surface to a maximum at the bed with no along-stream variation. Maximum values of τ_{uw} over 2-D dunes typically occur at, and just downstream, of the reattachment zone and along the shear layer. Large τ_{uw} values have been observed to extend downstream of the dune crest, defining the wake and the IBL below; τ_{uw} should tend toward zero (or even be slightly negative) moving up in the water column. Some authors have observed large Reynolds stresses in the IBL upstream of the dune crest [e.g., *Nelson et al.*, 1993]. However, others have failed to observe this pattern [*Bennett and Best*, 1995; *Venditti and Bennett*, 2000]. It is unlikely this phenomenon could be observed here using the ADV technology due to the size of the sampling volume.

[32] The turbulent kinetic energy per unit volume is calculated as

$$\mathrm{TKE} = \frac{1}{2}\rho_w\left(\overline{u'^2} + \overline{v'^2} + \overline{w'^2}\right), \tag{12}$$

where $v' = v_i - V$ and v_i is an instantaneous velocity. TKE represents the energy extracted from the mean flow by the motion of turbulent eddies [*Kline et al.*, 1967; *Bradshaw*, 1971]. TKE production involves interactions of the Reynolds stresses with mean velocity gradients and, ultimately, TKE dissipation occurs via viscous forces after being passed through the inertial subrange of the turbulence spectrum [*Tennekes and Lumley*, 1972]. Since most turbulence production occurs at the boundary [*Kline et al.*, 1967], TKE can be expected to be largest near the bed for the flat bed case and decrease toward the water surface. Over a 2-D dune, *Venditti and Bennett* [2000] indicated that elevated TKE values define the wake structure, and also showed TKE reaches a maximum at reattachment and elevated levels occur in the separation cell.

4. Mean and Turbulent Flow Field Over Flat and 2-D Dune Beds

[33] Contour maps of the mean and turbulent flow parameters are shown in Figures 4–8 and are discussed in detail below. Some local artifacts of the contouring process are evident in some plots (compare sinuous saddle and lobe U maps). Naturally, these could be smoothed by adjusting the grid spacing or adjusting contour intervals for individual maps. However, this would largely negate the direct comparison between maps and was not attempted.

4.1. Flat Bed

[34] Flow over the fixed flat bed was directly scaled to observations of flow over the active transport layer bed in the NSL experiments. Changes in the flow with the introduction of 2-D and 3-D bed forms form the primary observations presented herein. Thus it is of interest to ensure that the flow field over the flat bed compares well with the NSL experiments and theory.

[35] The mean velocity profiles of both the fixed flat bed and NSL experiments are log linear through the lower $0.2d$ and U_{rms} profiles decay exponentially away from the bed (Figure 9). The mean velocity profile is slightly steeper and U_{rms} is larger over the flat active transport bed in the NSL experiments. This is caused by form drag generated as nascent bed forms began to develop and is in accordance with the suggestion of *Best et al.* [1997] that the transport layer modulates turbulent flow by increasing roughness heights and near-bed turbulence intensities while reducing mixing lengths.

[36] Contour maps of U, W and the turbulence parameters over the flat bed show no along-stream variation (Figures 4–8), indicating the flow was indeed uniform. Near the bed (up to $\sim 0.33d$) $\tau_{uw} \approx 0.2$–0.4 Pa (Figure 7) and TKE ranged between 0.5 and 1.5 Pa closest to the bed (Figure 8). In the middle flow region, between ~ 0.33 and $0.66d$, τ_{uw} decreased toward zero and eventually became negative above $\sim 0.66d$, indicating the decoupling of u and w motions and the absence of significant momentum exchange. This can also indicate downward flow and the presence of secondary circulation. Figure 10 plots the vertical variation in spatially averaged W along the centerline and shows weakly downward flow over most of water column, except near the bed where there is clearly a vertical water flux. The vertical TKE distribution tends toward zero above $\sim 0.33d$ indicating there was little or no energy transfer from the mean flow (turbulence production) away from the bed. Overall, flow over the fixed flat bed behaved in the manner suggested by current conceptions of boundary layer flow [*Nezu and Nakagawa*, 1993] and was similar to flow over the active transport layer bed in the NSL experiments.

4.2. The 2-D Dunes

[37] Flow over the 2-D dunes displays most of the features described in previous research. Velocity profiles (Figure 9) and the U contour map (Figure 4) reveal that flow was generally decelerated over the dune trough and accelerated over the dune crest. Mean streamwise flow over the stoss slope of the 2-D dune was nearly identical to flow over the flat bed, but U_{rms} values were larger over the whole 2-D dune profile (Figure 9). A shear layer that extended from the slip face base to the first slope break (B2) is evident in the contour map and by the steep gradient in the mean velocity profile over the trough. I define a shear layer here as a steepened portion of the mean velocity gradient reflecting a change in velocity between two overlying flow regions. There was also an upstream directed flow near the slip face indicating flow separation (Figure 4). The region is not

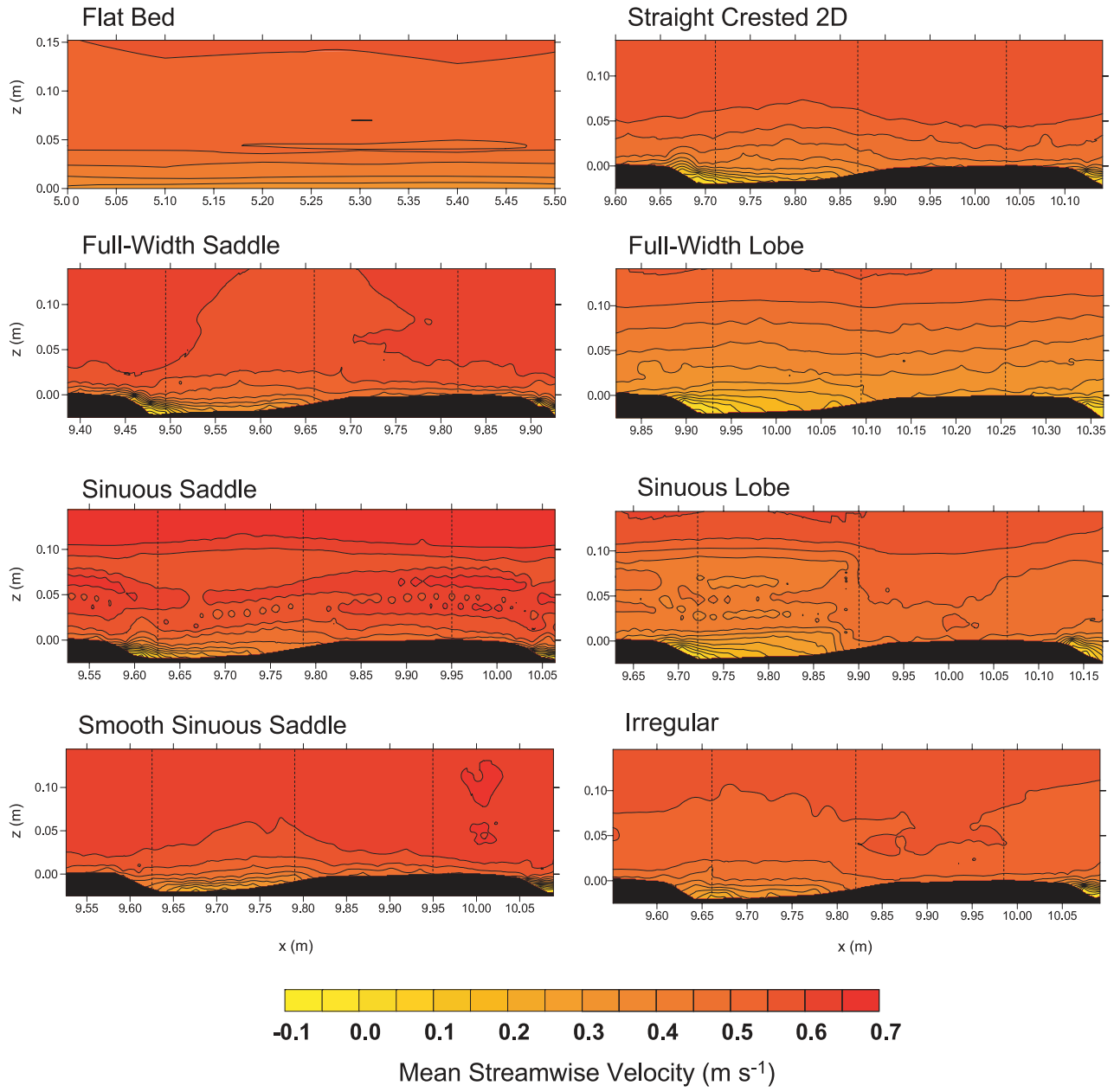

Figure 4. Mean streamwise velocity (z is height above the crest and x is distance along the flume). Note that after profiles were taken between x = 9.630 and 9.855 m over the sinuous lobe, the ADV probe was replaced by another probe which led to an apparent disruption in the pattern of U. Only the sinuous lobe measurements are affected. Flow is left to right. Dashed lines indicate locations of profiles shown in Figures 9 and 11.

large, but the exact configuration of flow in this region is difficult to resolve with an ADV.

[38] The W contour map (Figure 5) shows plunging vertical flow over the dune lee slope and flow directed toward the water surface between B2 and B1. Near the crest, mean vertical flow was negative (toward the bed). Streamwise spatial averages of W (Figure 10) show downward flow along the flume centerline, except just above the bed form crests where topographic forcing between B2 and B1 dominate the spatial average. Overall, the pattern suggests secondary circulation where flow moved away from the centerline as it approached the bed. The secondary circulation is stronger than over the flat bed indicating that the roughness offered by the 2-D dunes played a role in the secondary circulations.

[39] Plots of I_u, τ_{uw}, and TKE (Figures 6, 7, and 8, respectively) reveal a wake structure, particularly well defined by the I_u = 1.25 and TKE = 2 Pa isolines, that extended from the lee slope through the trough region and up over the downstream crest. Low I_u, τ_{uw}, and TKE values beneath the wake from the second stoss slope break (B1) to the crest and above $\sim 0.5d$ indicate the presence of an internal boundary layer and the outer flow layer, respectively. Reynolds stress reached a maximum ($\tau_{uw} \approx 1.0-$

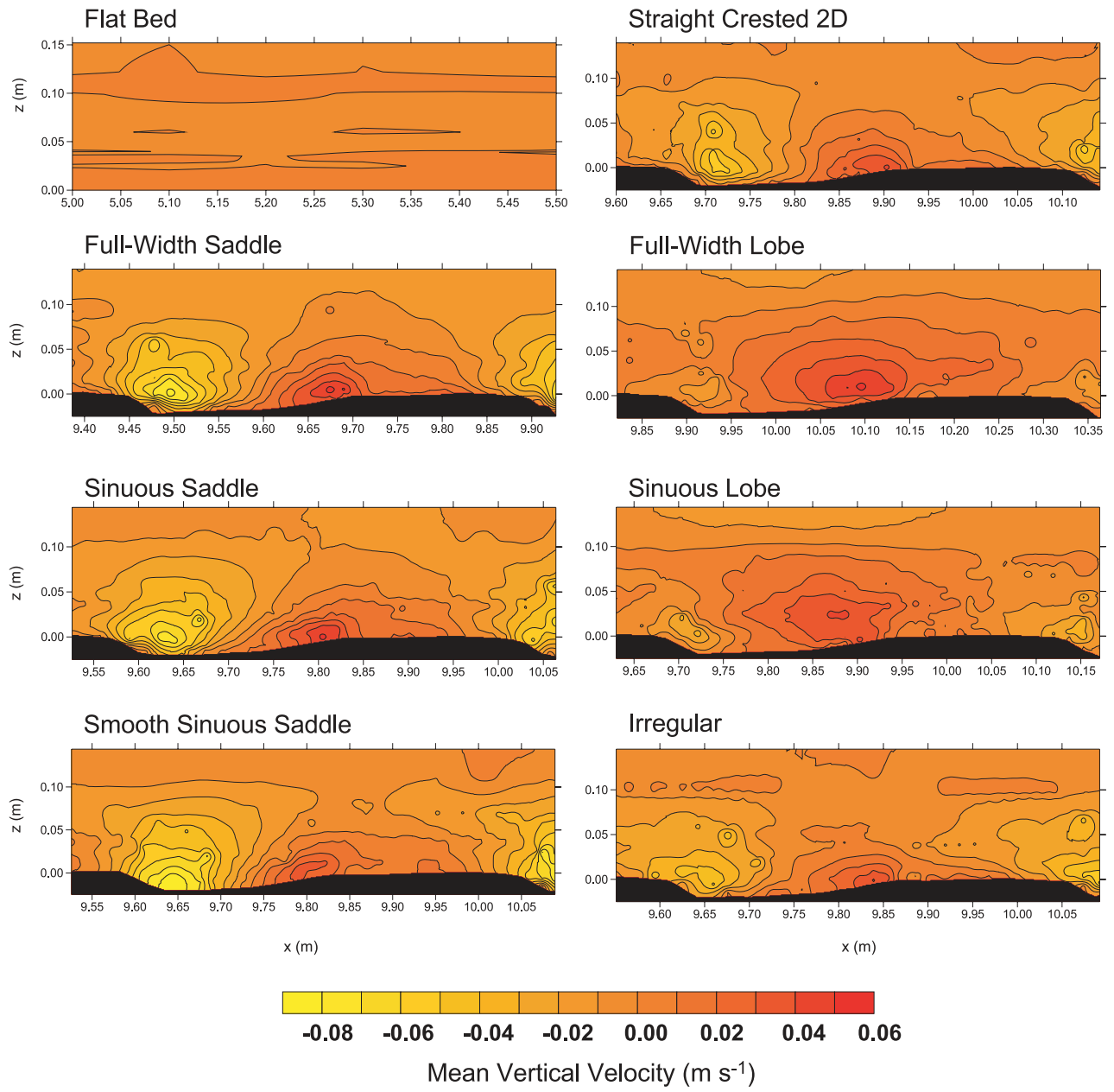

Figure 5. Mean vertical velocity (z is height above the crest and x is distance along the flume). Flow is left to right.

1.2 Pa) in the separation cell and was elevated through the trough region and wake structure. The reattachment point and IBL maximum stress were not observed in Figures 6, 7, and 8, but this is likely due to the limited resolution of the ADV.

[40] Overall, the shear layer, separation vortex, and wake structure over the 2-D dunes are less well defined than in previous studies [cf. *Venditti and Bennett*, 2000], which was probably caused by bed form shape. The along-stream profile of bed forms used in this study was created from a nondimensional model of observations from NSL experiments. The profile differs slightly from the bed forms used in previous work (see references above in Section 3) where the maximum elevation coincided with the slip face crest (often referred to as angle of repose dunes). In a study of flow over a low-angle dune, *Best and Kostaschuk* [2002] observed generally weaker, intermittent shear layer development and flow reversal than over angle of repose dunes, resulting in a lower velocity differential in the lee of the bed form. It is probable similar effects weakened the strength of flow separation, the shear layer, and wake over the 2-D dunes examined here. Nevertheless, the bed form shape used in this study is characteristic of bed forms in natural channels [*Best*, 2005a].

5. Mean and Turbulent Flow Fields Over 3-D Dune Beds

[41] Before proceeding with a discussion of the characteristics of flow over 3-D dunes, it is necessary to consider the

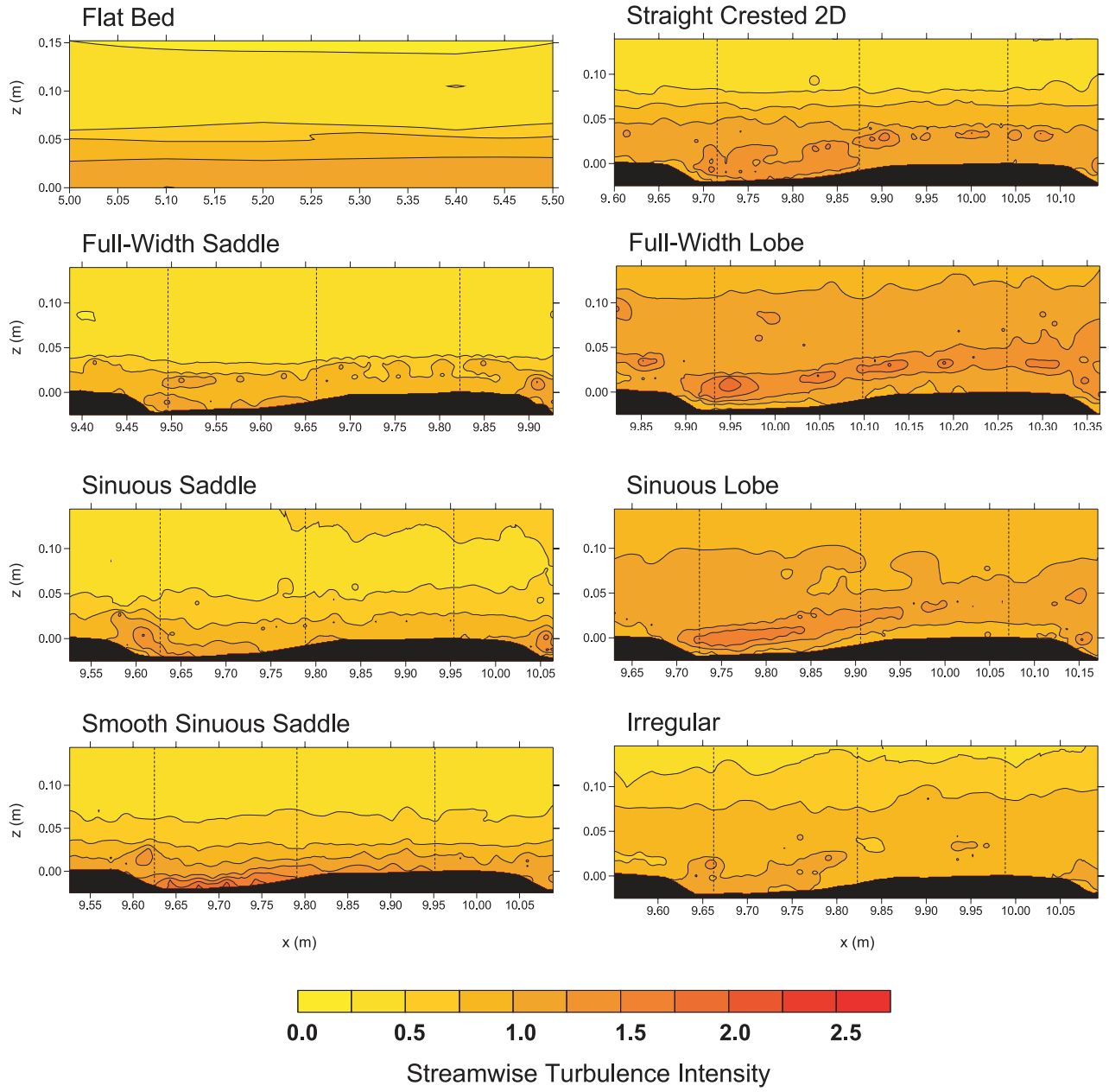

Figure 6. Streamwise turbulence intensity (z is height above the crest and x is distance along the flume). Flow is left to right. Dashed lines indicate locations of profiles shown in Figures 9 and 11.

effect of the jagged crest line on the flow structure which was tested by smoothing the SNS crest line and repeating that series of measurements (referred at as the SSS configuration). Figures 4 and 5 show the mean velocities (U and W) over the jagged and smoothed sinuous saddle configuration. The flow fields are remarkably similar, except that in the center of the saddle, where W was larger over the smoothed crest line, suggesting that the jagged crest suppressed downwelling in the trough. Figures 6, 7, and 8 show the turbulence quantities, which are also remarkable similar between the jagged and smooth sinuous saddle crest lines. Yet, the level of turbulence was somewhat larger in the trough of the jagged crest line due to the larger cross-stream roughness. Also, the suppression of downwelling into the trough over the jagged crest allowed turbulence to be transported higher into the water column. Nevertheless, the differences in the flow field over the jagged (SNS) and smoothed sinuous saddle (SSS) configurations are minor and not as great as the differences amongst the other 3-D configurations that are described below.

5.1. Full Width Lobe (FWL) and Saddle (FWS)

[42] The difference in the bulk hydraulics between the 2-D and FWL bed configurations was not great. Differences between d and $\overline{U}$ are on the order of the potential measurement error for these quantities. However, there was an increase in the water surface slope that resulted in a 14% increase in the total boundary shear stress (Table 1). Adjustments to the mean and turbulent flow field were more dramatic.

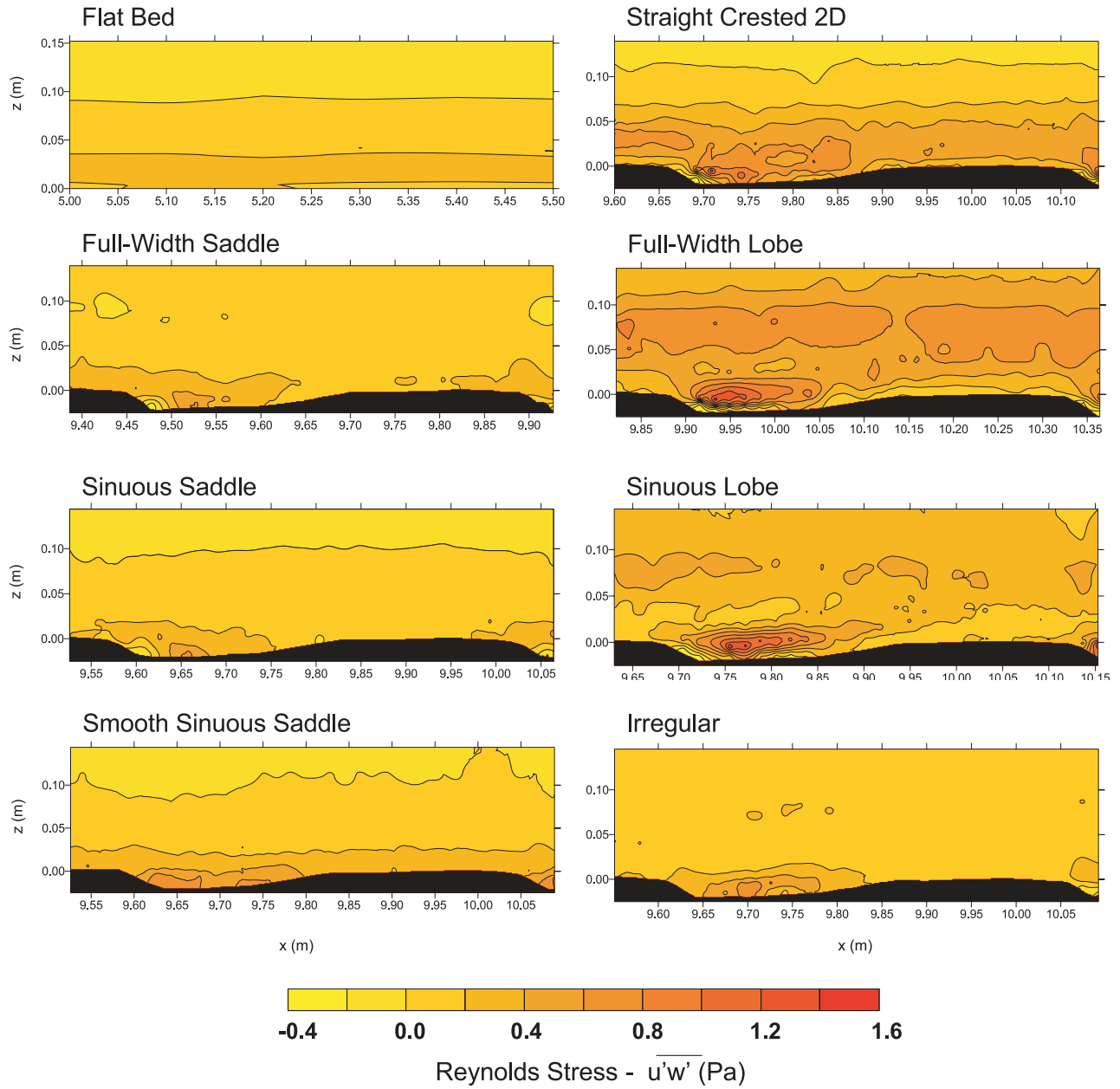

Figure 7. Vertical and streamwise components of the Reynolds stress (z is height above the crest and x is distance along the flume). Flow is left to right.

[43] Mean u profiles (Figure 11a) and the FWL contour maps of U (Figure 4) indicate that flow was retarded over the bed form, compared to the 2-D dune. There was a large decelerated flow zone in the trough and a distinct shear layer. An extensive zone where $U < 0$ occurred abutting the slip face, suggesting a stronger recirculation cell than over the 2-D dune. Vertical flow (Figure 5) was much weaker over the FWL dune than over the 2-D dune with plunging flow in the lee, but a strong and extensive vertical current occurred above B2–B1. A weak vertical flow component persisted downstream of this zone and even over the FWL dune crest. Streamwise spatial averages of W (Figure 10) show strong upward flow occurred over the FWL centerline which suggests strong secondary circulation where flow moved into the centerline near the bed as it moved away from the bed. The secondary circulation was stronger in magnitude than over 2-D dunes.

[44] Turbulence was enhanced over the FWL relative to the 2-D dune, partly because it was being transported into the center of the flume and upward by the secondary flow. Profiles of U_{rms} (Figure 11a) reveal larger turbulence intensity in the upper portions of the flow but similar values near the base, although U_{rms} was larger at the trough profile, owing to more vigorous mixing in the separation cell. Contour maps of I_u and τ_{uw} reveal low values in the upper and lower portions of flow with a strong core of elevated values that occupied $\sim 0.33d$. The wake structure, defined by the $I_u = 1.25$ and TKE = 2.5 Pa isolines, extended from the upstream lee slope downstream over the next dune crest, and was somewhat stronger than in the lee of the 2-D dune

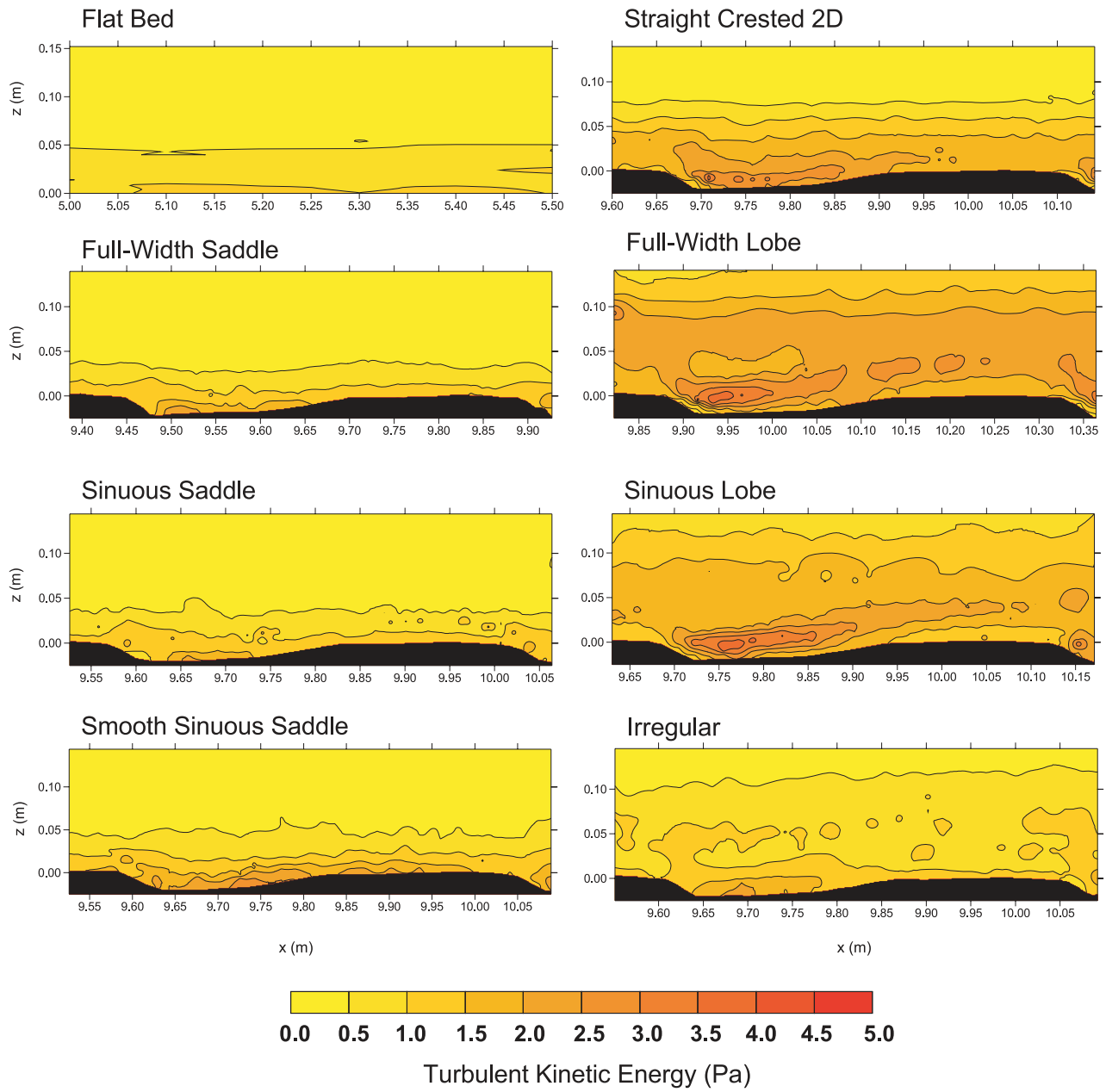

Figure 8. Turbulent kinetic energy per unit volume (z is height above the crest and x is distance along the flume). Flow is left to right.

(Figures 6 and 8). In fact, it is likely that the core of more turbulent flow was composed of stacked wakes from upstream bed forms as suggested by *Nelson and Smith* [1986]. Low I_u, τ_{uw}, and TKE values indicate there was an IBL beneath the wake on the stoss slope that was thicker than over the 2-D dune (Figures 6, 7, and 8). The separation cell appears as a well-defined elongated zone where τ_{uw} exceeds 0.6 Pa.

[45] Differences in the bulk hydraulics between the 2-D and FWS dune configurations were more substantial than between the 2-D and FWL dune configurations. There was an increase in d and a decrease in $\overline{U}$ that exceeded the potential measurements errors and the water surface slope increased substantially (Table 1). This resulted in a 38% increase in the total boundary shear stress relative to the 2-D dune. As over the FWL configuration, there were adjustments to the mean and turbulent flow field caused by the 3-D shape.

[46] Mean u profiles (Figure 11a) and the FWS contour map of U (Figure 4) indicate larger velocities over the dune profile relative to the 2-D dune. There is some evidence of a shear layer in the U profile over the trough, but it was not as pronounced as over the 2-D dune and diminished greatly ~1 step height downstream of the slip face crest. The U contour map suggests a low-velocity zone where $U < 0$ occurred immediately adjacent the lee slope, however, this zone was not extensive. The W contour map indicates a strong plunging flow occurred over the dune lee slope and a responding surface directed flow between the slope breaks (B2 and B1). The strength of these vertical flow compo-

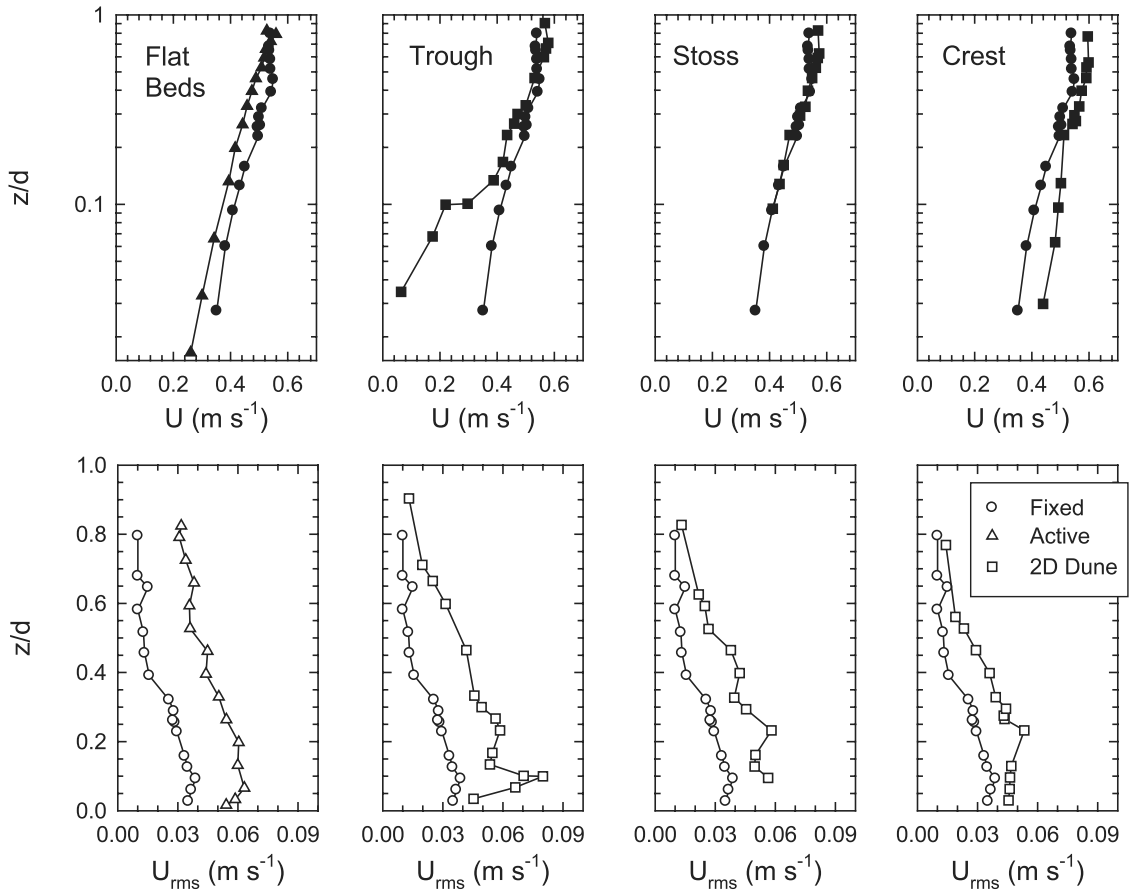

Figure 9. Select profiles of mean streamwise velocity U (solid symbols) and streamwise root-mean-square velocity U_{rms} (open symbols) over the flat bed and the 2-D dune configuration. Flat bed data were collected during flow strength B [see *Venditti et al.*, 2005b] with active transport in the NSL experiments and over the fixed flat bed without transport. The fixed flat bed profile was taken at 5.0 m and is the same for trough, stoss, and crest. The datum for all the 2-D dune data is the dune surface. See Figures 4 and 6 for exact profile positions over the 2-D dune.

nents was stronger than over the 2-D dune. Vertical flow over the crest was negligible. Streamwise spatial averages of W (Figure 10) show strong downward flow occurred over the FWS centerline which suggests secondary circulation moving in the opposite direction than over the FWL bed forms. Secondary flow was similar to that over the 2-D dunes, moving away from the centerline as it approached the bed, but of greater magnitude.

[47] Turbulence was suppressed over the FWS bed form, partly because turbulence was being transported away from the centerline near the bed by the secondary flow. This is demonstrated by comparison of the 2-D dune and FWS contour maps of I_u, τ_{uw}, and TKE (Figures 6, 7, and 8) as well as profiles of U_{rms} (Figure 11a) that reveal diminished turbulence intensity in the center core of the flow. Turbulence levels were larger in the lower 0.5d than the rest of the flow field, but generally less than over the 2-D bed form. Interestingly, there is no apparent wake structure and consequently no observable IBL in any of the contour maps. The separation cell was small, absent, or only weakly defined. I_u, τ_{uw}, and TKE were somewhat larger in the trough area bounded by SFC upstream and B1 downstream, suggesting some turbulence was generated over the dune but not on the scale of the 2-D or FWL dune.

5.2. Sinuous Lobe (SNL) and Saddle (SNS)

[48] There is one common set of bulk hydraulic parameters for the sinuous crest (lobe and saddle) configuration (Table 1). The difference between the mean flow depth and velocity between the 2-D and sinuous bed form configurations was larger than between the 2-D and full width bed forms. Flow depth over the sinuous-crested bed forms was 4 mm (5 mm for the smoothed crest line) larger and flow velocity was 14 mm s^{-1} (18 for the smoothed crest line) smaller than over the 2-D dune (Table 1). Water surface slope was nearly identical over the 2-D, sinuous jagged, and sinuous smooth crest lines. As a consequence, the difference in total boundary shear between the sinuous bed forms and the 2-D features did not exceed the associated potential error. Changing the bed form crest line from 2-D to 3-D had a larger effect on flow resistance than whether the bed form crest line was smooth or jagged.

[49] Qualitatively, the sinuous features behaved as the full width ones. Flow velocities were lower over the SNL and higher over the SNS configurations than over the 2-D dune

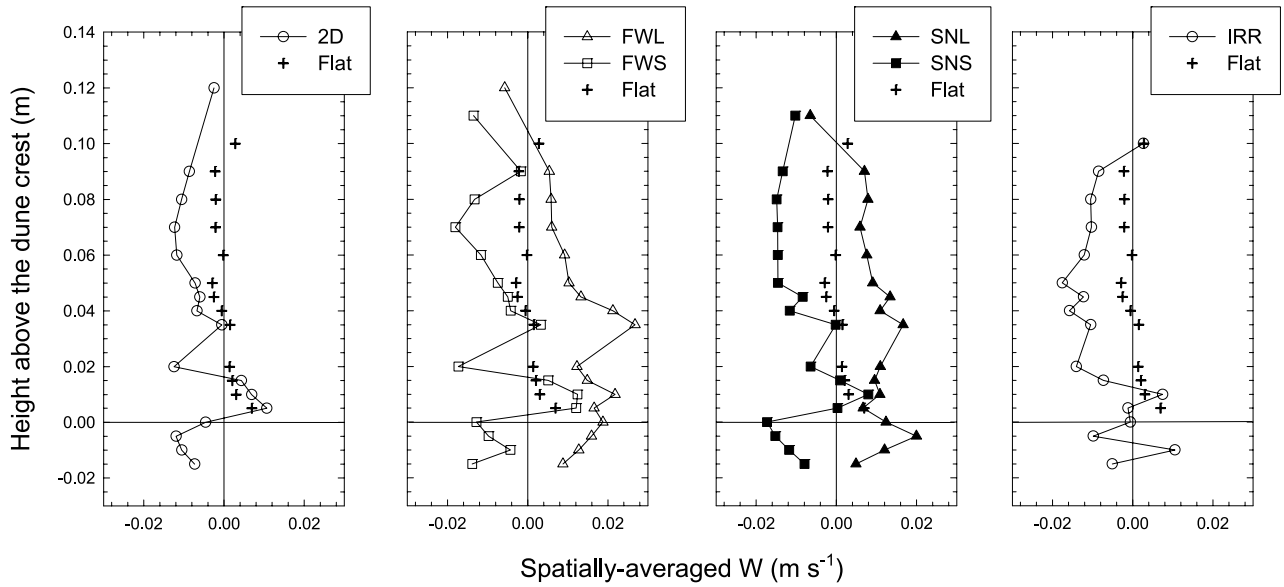

Figure 10. Along-stream spatial averages of centerline mean vertical velocity *W*. Spatial averages are along lines of constant elevation above the bed form crest.

(Figure 4). However, the magnitude of the deviation was not as large as between the 2-D and full width bed forms (Figure 11b). The shear layer over the saddle was not strong, yet a strong shear layer existed in the lee of the lobe, consistent with observations over the full width bed forms (Figure 11b). Contour maps of U (Figure 4) indicate that there was a large decelerated zone over the sinuous lobe and negative U velocities occurred near the SNL lee slope. Over the SNS, the decelerated zone was quite limited, and there were no negative values of U observed.

[50] Contour maps of W indicate that plunging flow occurred with a surface-directed return flow at B1 over both the sinuous lobe and saddle (Figure 5). Over the crest of the sinuous lobe, vertical flow was negligible, while over the sinuous saddle crest flow was directed toward the bed. Figure 5 shows that magnitudes of the plunging and return flows were similar over the sinuous and full width bed forms, suggesting vertical flow was not strongly affected by the cross-stream scale of the features. However, profiles of W spatially averaged along the centerline (Figure 10) provide evidence of secondary flow patterns over the sinuous lobe and saddle in the same directions as over the full width bed forms but of slightly lesser magnitude.

[51] The characteristics of the turbulent flow over the sinuous bed forms also bear strong similarity to the full width bed forms. Turbulence was enhanced over the lobe and suppressed over the saddle. Over the SNL, the upper portion of the U_{rms} profile was larger than over the 2-D dune (Figure 11b) and contour maps reveal a central core region that had larger I_u and τ_{uw} values compared to flow above and below (Figures 6 and 7). This region was less pronounced over the sinuous lobe when compared to the FWL. The wake structure is well defined by the $I_u = 1.25$ and TKE = 2.0 Pa isolines and was better defined over the sinuous lobe than over the full width lobe, suggesting the lesser width concentrated the strength of the wake (Figures 6 and 8). The central core was not as turbulent as over the full width lobe because of the neighboring saddle that had no observable wake. Low values of I_u, τ_{uw}, and TKE indicate that there was an IBL beneath the wake on the stoss slope of the sinuous lobe that was similar in thickness to the IBL over the full width lobe. The separation cell was quite pronounced over the sinuous lobe trough where $\tau_{uw} \approx 1.4$–1.6 Pa and was of similar magnitude to that associated with the full width lobe.

[52] Over the sinuous saddle, turbulence was suppressed in the central core of the flow, but similar U_{rms} values occurred at the top and base of the profiles (Figure 11b) as over the FWS. The flow separation cell was weakly defined; τ_{uw} reached a maximum of only $\sim$0.6 Pa (Figure 7). Similarly, the wake structure was absent or weakly developed and, consequently there was no apparent IBL.

5.3. Irregular (IRR) Crest

[53] Differences in the bulk hydraulic parameters between the 2-D and irregular bed form orientations were substantial. Mean flow depth was 6 mm greater and mean flow velocity was 20 mm s^{-1} less than over a 2-D dune. The water surface slope was also lower than over the 2-D dune resulting in a 20% reduction in the total boundary shear stress.

[54] Profiles over the irregular dune were taken where the neighboring crests were staggered upstream and downstream forming an asymmetric lobe in the flume center (Figure 3). Profiles of U over irregular and 2-D dunes were identical above the dune height, but below this point U was larger than over the 2-D dune morphology, although a strong shear layer was observed (Figure 11c). The reduction in U was quite minimal in the trough zone and no upstream directed flow was observed (Figure 4). The pattern of W velocities was similar over the irregular and the 2-D dunes (Figure 5). Plunging flow occurred over the dune crest with an upward directed return flow at B1. There was a mean cross-stream velocity over the asymmetric lobe where

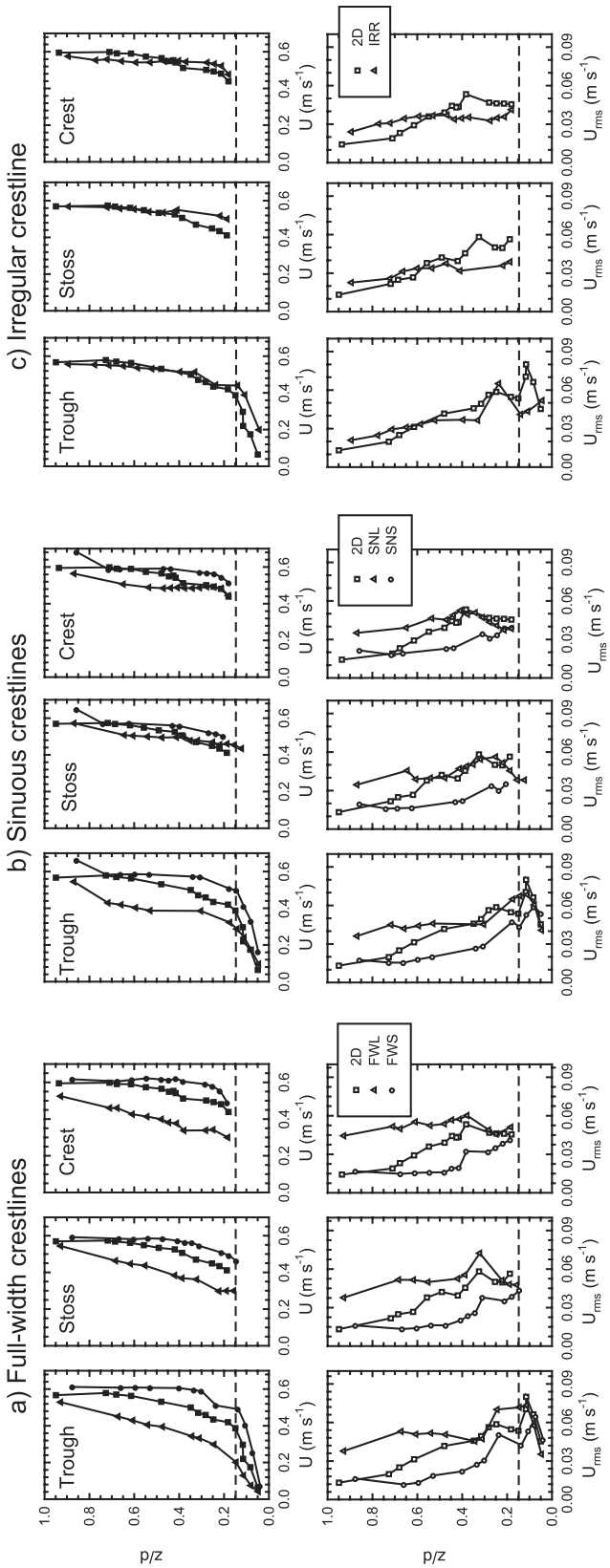

Figure 11. Select profiles of mean streamwise velocity U (solid symbols) and streamwise root-mean-square velocity U_{rms} (open symbols) over (a) the full width lobe (FWL) and full width saddle (FWS), (b) sinuous lobe (SNL) and sinuous saddle (SNS), and (c) irregular (IRR) configurations. Profiles over the 2-D dune configuration are plotted for comparison; z is height above the dune trough and is normalized by the mean flow depth d. The dashed line is the crest height. See Figures 4 and 6 for exact profile positions over the 3-D dunes.

the velocity measurements were taken, especially in the dune trough where $V = 0.08$ m s^{-1} at the bed in one location [see *Venditti*, 2003]. There is a prominent downward flow component evident in profiles of streamwise spatial averages of W (Figure 10), suggesting secondary circulation where flow was moving away from the centerline as it approached the bed.

[55] A wake, IBL, and separation cell appeared to have developed over the irregular dunes. However, there was a zone of more turbulent flow, observable in τ_{uw} and TKE contour maps, in the bed form trough, which means some separation induced mixing must have occurred (Figures 7 and 8). Turbulent intensities were moderately larger in the outer layer over the irregular dune than over the 2-D dune configuration, but near the bed, I_u was much less (Figure 6).

6. Discussion

6.1. Effect of 3-D Morphology on Momentum Exchange, Energy Transfers, and Near-Bed Velocity

[56] Over a flat bed, momentum exchange and mixing decrease with distance from the bed while energy transfer from the mean flow is confined to the lower $0.33d$. The presence of a 2-D dune alters these distributions. The separation cell dominates momentum exchange but mixing is also strong along the wake layer. As over a flat bed, little mixing occurs between $0.66d$ and the surface. Similarly, the wake structure and separation cell dominate energy transfer from the mean flow. Introduction of three dimensionality to the 2-D crest line changes these distributions and the flow structure by inducing secondary flow and altering energy transfers from mean to turbulent flow. The secondary circulation cells setup by the bed topography were well documented in the work by *Maddux et al.* [2003a, 2003b] and measurements of this type were not pursued in this work. However, the influence of these secondary currents is evident.

[57] Mean flow over a lobe is decelerated, relative to a 2-D dune, and there is a net upward flux of water (Figure 12a) indicating fluid is transported away from the centerline by secondary flow (Figure 12b). The enhancement of the mean velocities along the centerline of the FWL with negligible changes in $\overline{U}$ demands that there be compensating cross-stream fluid motions toward the centerline near the bed. This general pattern of secondary circulation is also evident in along-stream, spatial averages of mean vertical velocity that show upward flow occurred at nearly all levels over the FWL and SNL bed form centerline (Figure 10). Mean flow over a saddle is accelerated, relative to a 2-D dune, and there is a net downward flux of water (Figure 12a) indicating fluid is transported away from the centerline by secondary flow near the bed (Figure 12b). The reduction in local mean velocity along the centerline of the FWS, with negligible changes in $\overline{U}$, indicates compensating cross-stream fluid motions away from the centerline. There is a near-bed upward flux of water over the dune trough, caused by topographic forcing of the dune, but spatial averages of vertical velocity reveal downward flow occurred at nearly all levels over the FWS and SNS bed form centerline (Figure 10). This pattern of secondary circulation suggests that flow must converge in the lee of a lobe and diverge in the lee of a saddle (Figure 12c). *Allen* [1968] has shown that flow paths diverge over lobe shapes and converge over saddle shapes, roughly perpendicular to lines of equal elevation. The data presented here do not rule out the possibility that this is also occurring here, although it would need to be a local effect as flow approaches the crest (Figure 12c).

[58] Over the full width bed forms, the downward mean velocity over the saddles, and upward velocity over the lobes, suggest two circulation cells exist on either side of the centerline. Since flow patterns over the sinuous lobe and saddle formation are identical to flow over the full width formations, the secondary circulation produced over the sinuous bed must have a lateral length scale half that of the full width case. Thus four circulation cells must exist as diagrammed Figure 12b.

[59] The pattern of flow in the x-z plane (Figure 12a) dictates the strength of the separation cell and the associated wake structure. As flow approaches the lobe crest, mean flow paths strongly diverge along a shear layer that develops between upwelling flow over the crest and downward directed flow into the separation cell. The divergence in the mean flow paths at the separation point near the dune crest forms a stronger and larger separation cell than over a 2-D dune, and a wake structure with vigorous mixing. As flow over a lobe moves downstream of separation, the upwelling flow carries turbulence vertically, advecting turbulent energy and momentum high into the flow field (Figure 12a). Mean flow over a saddle plunges over the trough due to secondary circulation which suppresses the strong divergence of mean flow paths observable over a lobe. As such, the development of the separation cell and wake structures are suppressed. Lacking a strong upwelling flow over the stoss slope, vertical flux of turbulence is not as strong over a saddle as over a lobe and the overall level of turbulence is lower (Figure 12a).

[60] The decrease in mean velocity over lobes and increase over saddles is also conditioned by energy transfers from mean to turbulent flow. Over a lobe shape, the vigorous mixing that occurs in the wake and flow separation cell causes greater transfers of mean flow energy to turbulence, reducing the mean flow velocity. Development of a strong flow separation cell and wake does not occur over the saddle. As such, exchange of energy from the mean flow and momentum exchanges are limited, and consequently, the mean flow is stronger than over a lobe.

[61] In natural channels, the bed morphology may be dominated by either channel-wide saddles or lobes, but a common bed configuration is one where a saddle shape is coupled with a downstream lobe and vice versa [cf. *Venditti et al.*, 2005a; *Parsons et al.*, 2005]. This morphology is pattern stable, but is constantly rearranging [*Venditti et al.*, 2005a]. Saddles tend to be locations of intense erosion and downstream transport while lobes are largely depositional features. The observation of higher levels of turbulence over lobes compared with saddles in this study may seem counterintuitive as a coupling between the level of turbulence and erosion might be expected. However, over the stoss slope of bed forms downstream of a saddle, the dune back is exposed to higher velocity flow because of the absence of strong flow separation and an internal boundary layer. This increases the near-bed velocity gradient and local shear stress, causing the intense erosion near the crest and

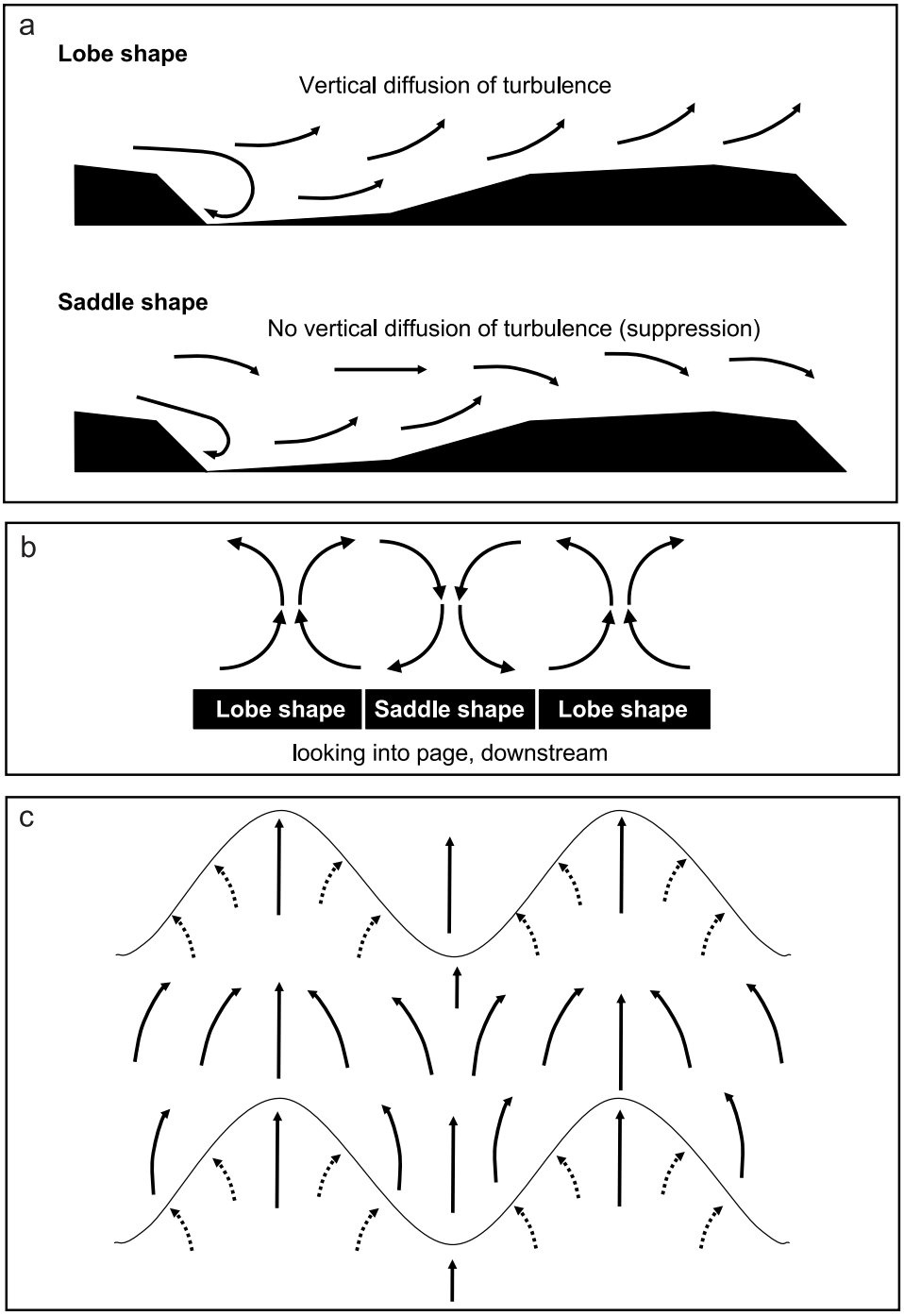

Figure 12. Divergence and convergence of mean flow over lobe and saddle crest lines in the (a) *x-z* plane, (b) *y-z* plane (averaged over one dune length), and (c) *x-y* plane (near the bed). The dashed arrows in Figure 12c indicate patterns observed in experiments by *Allen* [1968], and the solid arrows are consistent with the present experiments.

deposition further downstream into a lobe. Bed forms downstream of a lobe are buffered from the mean flow by the wake and internal boundary layer. The flow velocities near the bed are not as strong as over a saddle, resulting in smaller near-bed velocity gradients and local shear stresses. This starves the downstream dune of sediment, promoting a downstream saddle. Nevertheless, it is not clear from the present data set why an intensely turbulent mixing cell was not observed in the lee of saddles, given the common observation of vigorous stirring of sediment in saddle troughs. Spatially resolved, time dependant observations of flow in the lee of active 3-D sand dunes are required to examine this further.

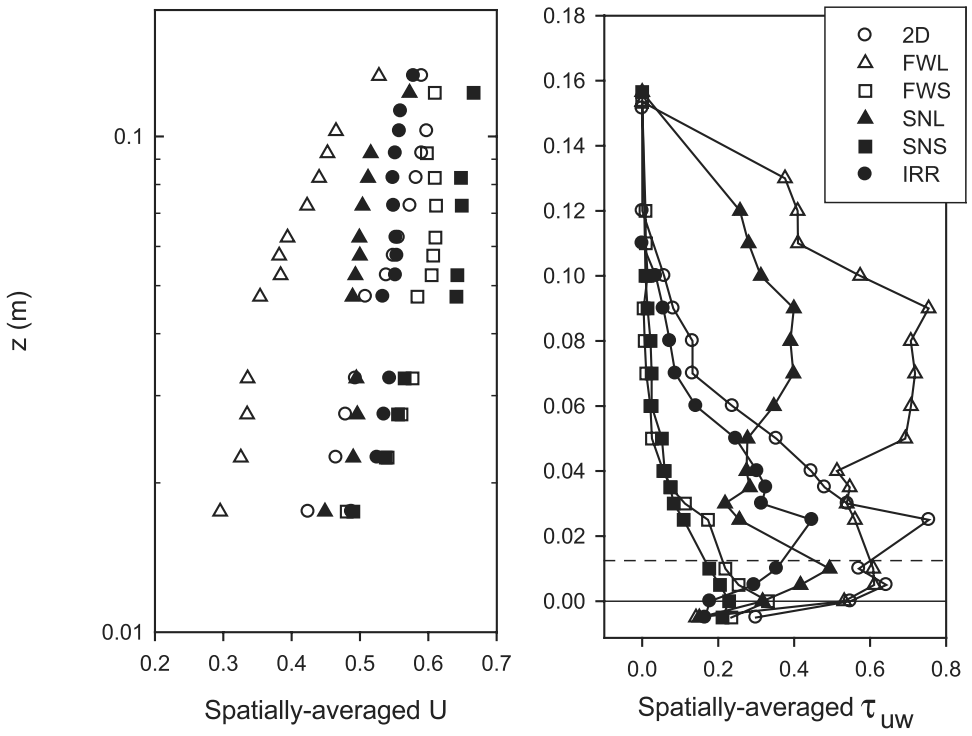

Figure 13. Along-stream spatial averages of centerline mean velocity and Reynolds stress. Spatial averages of velocity and Reynolds stress are along constant heights above the mean bed elevation, $H(1-\beta)$ above the dune trough (10 mm). Velocity averages include only those measurements over the dune stoss slope, which excludes data in the separation cell as recommended by *McLean et al.* [1999]. Reynolds stress averages include data between successive crests, including the separation cell. Reynolds stress profiles are forced to zero at the water surface. The dashed line is the crest height.

6.2. Flow Resistance of 2-D and 3-D Bed Forms

[62] There are a variety of methods proposed to calculate flow resistance (total boundary shear stress) from measured flow data including spatially averaging velocity profiles [*Smith and McLean*, 1977; *McLean et al.*, 1999], spatially averaged Reynolds stress profiles [*Nezu and Rodi*, 1986; *Lyn*, 1993; *McLean et al.*, 1999], and double-averaged (in space and time) versions of the momentum equations [*Maddux et al.*, 2003b]. *McLean et al.* [1999] examined the segmented profile method for shear stress determination proposed decades earlier by *Smith and McLean* [1977] for use with spatially averaged, logarithmic velocity profiles. *McLean et al.* [1999] concluded the segmented method, where the outer profile is the total boundary shear stress and the inner profile is bed shear stress, is only accurate to ±30%, which is not a great improvement over just using linear logarithmic fits to a velocity profile which is accurate to ±45%. *McLean et al.* [1999] suggest use of a spatially averaged Reynolds stress profile extended to the mean bed level as a better method, but more recent work by *Maddux et al.* [2003b] suggests this cannot be done for flow over 3-D dunes and instead used double-averaged (in space and time) versions of the momentum equations.

[63] I attempted to use logarithmic velocity profiles, segmented logarithmic velocity profiles, and spatially averaged Reynolds stress profiles to determine the total boundary shear stress over the flat and 2-D dune beds and reasonable values can be obtained with both methods. However, streamwise averages of centerline velocity and Reynolds stress over the 3-D dunes examined here produce a wide variety of profile shapes (Figure 13), and it is not obvious how total boundary shear stress values can be reliably obtained using objective methods for each profile. Unfortunately, spatial averages of the momentum equation over laterally variable topography require multiple streamwise flow field transects at various cross-stream positions (as in the work by *Maddux et al.* [2003a, 2003b]), which are not available. If these data had been available, it is likely that both the spatially averaged velocity and Reynolds stress plots would yield similar shear stress estimates. Fortunately, the total boundary shear stress can be obtained from the depth-slope product, but partitioning that stress into its components parts (skin stress, form stress, form-induced stress) cannot be pursued.

[64] Figure 14 plots the total boundary shear stress (τ) for each bed configuration with error bars derived from propagated errors in the slope and flow depth. Comparison of τ over the 2-D bed to its value over the 3-D beds reveals that three dimensionality can increase or decrease flow resistance. It can be argued that a drag coefficient should be compared rather than τ, but since the channel discharge and bed form relief were held constant, and uniform flow was always maintained, changes in τ are entirely due to changes in the bed form crest line shape. Nevertheless, the drag coefficients found in Table 1 display the same patterns in flow resistance.

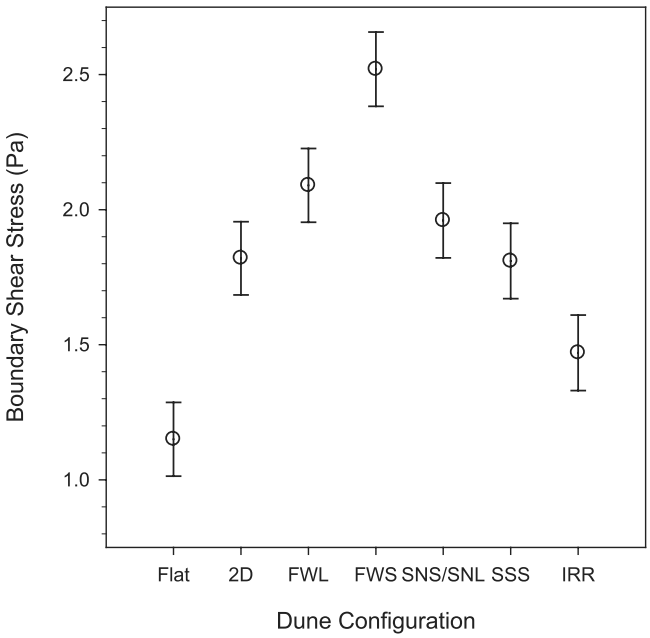

Figure 14. Variation in total boundary shear stress with crest shape. Error bars are calculated by propagating uncertainty derived from flow depth and bed slope measurements.

[65] FWL and FWS bed forms had 14 and 38% larger τ than the 2-D dune, respectively. *Maddux et al.* [2003a] found that flow resistance over their quasi-3-D bed forms was 78% greater for shallow flow (relative roughness $d/H \approx 4$) and 37% greater in deeper flow ($d/H \approx 14$) when compared to similarly scaled 2-D dunes. Results for the FWL and FWS bed forms generally agree with their result in so far as 3-D dunes increase flow resistance.

[66] *Maddux et al.* [2003a] attributed the differences in drag over 2-D and 3-D bed forms of the same size to an asymmetry in the distribution of near-bed velocities over the quasi-3-D forms, caused by topographic steering with higher near bed velocities contributing to greater skin and form drag in a nonlinear fashion. This is a better explanation for the increase in drag in the experiments of *Maddux et al.* [2003a], because the bed forms had variable heights and wavelengths. In general, and especially in the present experiments, where the bed form height and length were constant, the strength and the extent of flow separation controls flow resistance, so most of the changes in drag are caused by variation in the magnitude of form drag.

[67] In light of this, it is somewhat unexpected that an increase in τ occurred for both lobes and saddles. It is reasonable to expect that lobes would have higher flow resistance than a 2-D bed owing to the enhanced flow separation and that a saddle would have lower flow resistance because of the diminished flow separation. In fact, the velocity gradient, which is proportional to shear stress over flat beds and Reynolds stress profiles, does reflect a correlation between turbulence level and flow resistance (see Figure 13) over the full width bed forms. An earlier analysis [*Venditti*, 2003] based on these profiles returned the result that boundary shear stress and flow resistance are larger over lobes and smaller over saddles when compared to the 2-D dune, although this was done using segmented logarithmic velocity profiles and spatially averaged Reynolds stress profiles, which was not appropriate [*McLean et al.*, 1999; *Maddux et al.*, 2003b].

[68] The explanation of the observed increase in τ for both beds lies in the nature of the bed forms in the flume. A full width saddle was composed of a saddle shape in the center of the channel, but two half lobes at the sidewalls, while a full width lobe was composed of a centerline lobe and two half saddles at the smooth sidewalls (Figure 3). If the sidewalls were frictionless, the FWS and FWL configurations would have yielded exactly the same τ result. Over the FWS, flow was forced into the sidewall over the half lobes near the bed, forming lanes of slower moving fluid at the walls, increasing the sidewall effect. This should have increased flow resistance relative to a 2-D dune, even if the saddle was acting to reduce local drag in the center of the channel. Over the FWL, flow was drawn away from the sidewalls over the half saddles, forming lanes of faster moving fluid at the wall, which would have diminished the sidewall effect. Thus, even though both configurations were composed of two saddles and lobes, the proximity of the sidewalls and either the half lobes or half saddles unequally influenced total shear stress. Whether this unequal influence on flow resistance affected the patterns of flow along the channel centerline is not clear from the available data, but the bulk mean velocity is the same over the FWL and FWS bed configurations, suggesting that the overall effect on flow patterns is not great.

6.3. Drag Reduction and 3-D Bed Forms

[69] Flow resistance over the sinuous-crested bed forms was essentially the same as over the 2-D features, and the irregular shaped bed form field offered ~20% less resistance to flow than the 2-D and sinuous-crested dunes. Combined, these results suggest that the complexity of the bed form crest line affects how 3-D morphology impacts flow resistance. This stands in contrast to the result for simple 3-D bed forms (FWL, FWS, sinuous) examined herein and the results of *Maddux et al.* [2003a].

[70] Over the sinuous-crested dunes, where lobes and saddles were more tightly spaced than over the full width bed forms, diminution and enhancement of flow separation over the saddle and lobe appear to counteract upon the total flow resistance. For the irregular crest line, the complexity and asymmetry of the lobes and saddles prevent a simple summation of their effects on flow resistance to explain the drop in flow resistance. However, an explanation for the observed drop in drag may lie in the work of *Sirovich and Karlsson* [1997], who demonstrated a reduction in drag by changing arrangements of skin friction elements. They argued that a regular arrangement of skin roughness elements enhanced boundary layer bursting processes and drag, while an irregular arrangement broke up the bursting cycle, reducing drag.

[71] The straight-crested 2-D dunes and the sinuous-crested bed forms studied here are rough analogues of aligned pattern roughness elements used by *Sirovich and Karlsson* [1997] and indeed, these beds did enhance turbulence and drag compared to a flat bed, as might reasonably be expected. The irregular-crested dunes are analogues of random patterns of roughness elements. In accordance with

this analogy, there is a lower level of turbulence over the irregular-crested bed forms when compared to the simple regular crest line shapes and a consequent reduction in flow resistance. This is reflected in the absence of flow separation and wake development along the centerline.

[72] Similar reductions in the level of turbulence with a transition between 2-D and 3-D bed forms have been obtained by *Schindler and Robert* [2005], who examined changes in the flow structure at three points above an active sand bed as it transformed from ripples to 2-D dunes to 3-D dunes. *Schindler and Robert* [2005] observed that turbulence intensities and Reynolds stress decline with the transition between 2-D and 3-D dunes, yet total boundary shear stress increased in their experiments. They interpreted the decline as resulting from changes in the types of turbulent events generated, although as in the present study, the decline was likely also conditioned by the onset of secondary flow.

[73] The decline in drag observed in the present study cannot be fully explained by the onset of secondary circulation. Secondary flow is not significantly different over the IRR bed form compared to other morphologies (Figure 10), so some change in the generation of turbulence must also have occurred. Thus the lower level of turbulence observed in the present experiments supports the idea that nonuniformity in the cross-streamflow structure can reduce drag by altering the turbulent flow field as in the work of *Sirovich and Karlsson* [1997].

7. Summary and Conclusions

[74] Bed form three dimensionality significantly alters the flow field commonly observed over 2-D dunes. Lobe-shaped dune crest lines have a better defined wake structure and more vigorous mixing in the separation cell than observed over 2-D dunes. There is a vertical divergence of mean flow and upward directed secondary flow that enhances the level of turbulence. Saddle-shaped dune crest lines have a poorly developed separation cell and the wake does not appear to be a significant component of the flow field. Mean flow lines converge vertically with a net downward directed flow over saddles suppressing the level of turbulence. Qualitatively, the flow structure over lobes and saddles is roughly the same whether the bed forms occur across the entire flume or are in a sinuous configuration.

[75] Flow patterns over 3-D dunes demonstrate why in-line paired lobes and saddles occur. Near-bed velocity gradients are greater over saddles than over a 2-D dune, which will enhance sediment supply to a downstream lobe. Consequently, more mean flow energy is transferred to turbulence over the lobe, reducing near bed velocity gradients and sediment supply. This starves the downstream bed form of sediment and encourages the development of a saddle.

[76] Assuming that flow resistance is controlled by the extent and magnitude of flow separation, flow resistance over saddle-shaped bed forms should be lower than over a 2-D dune and higher over a lobe. Examination of the total flow resistance did not reveal this pattern, but it is likely that the bed form configuration in the channel conditioned this result. Interestingly, a bed form with irregularly spaced lobes and saddles of different sizes reduced flow resistance by 20% compared to straight-crested 2-D and sinuous-crested dunes. This change in flow resistance occurred due to a reduction in the level of turbulence over the dune. The observations presented here suggest flow resistance calculations in open channel flows need to consider the crestal shape bed forms because differently shaped bed forms with the same size can offer different levels of flow resistance. A single drag coefficient is thus inadequate in calculations where the bed can evolve through 2-D, 3-D and irregular 3-D bed form states.

Notation

A	bed form cross-sectional area.
d, $\overline{d}$, $d_{\max}$, $d_{\min}$	flow depth, its mean, maximum and minimum.
f_n	Nyquist frequency.
Fr	Froude number.
g	gravitational acceleration.
I_u	streamwise turbulence intensity.
H	dune height.
L	dune length.
L_c	distance along bed form crest.
L_y	distance between endpoints of bed form crest.
n	number of observations.
NDS	crest line nondimensional span.
Q	channel discharge.
r_{ADV}	ADV correlation coefficient.
Re	Reynolds number.
S	water surface and bed slope.
TKE	turbulent kinetic energy.
u, u_i, u', U	streamwise velocity, its instantaneous value, its fluctuation about the mean and its at-a-point, time-averaged mean.
$u*$	shear velocity based on the depth slope product.
$\overline{U}$	mean flow velocity.
U_{rms}, W_{rms}	streamwise and vertical at-a-point root-mean-square velocity.
w, w_i, W, w'	vertical velocity, its instantaneous value, its time-averaged mean and its fluctuation about the mean.
y_w	flume width.
$z_{WS-\max}$, $z_{WS-\min}$	maximum and minimum water surface level.
β	bed form shape factor.
φ, ϕ, γ	rotation angles.
ν	kinematic viscosity.
ρ_w	density of water.
τ	shear stress based on the depth slope product.
τ_{uw}	time-averaged at a point Reynolds stress.

[77] **Acknowledgments.** The research was supported by a Natural Science and Engineering Research Council of Canada (NSERC) operating grant to M. Church. Financial support to the author came through a UBC University Graduate Fellowship, a NSERC Post-Graduate Scholarship and an NSERC supported Research Assistantship. C. Christie and J. Rempel aided in the data collection in the Civil Engineering Hydraulics Laboratory at UBC with some help from N. Manklow. A. Vigna helped prepare some of the diagrams. The manuscript has benefited by the constructive reviews

of M. Church, M. Lamb, J. Best, and S. McLean, as well as discussions with P. Nelson.

References

Allen, J. R. L. (1968), *Current Ripples*, Elsevier, New York.

Baas, J. H. (1994), A flume study on the development and equilibrium morphology of current ripples in very fine sand, *Sedimentology*, *41*, 185–209.

Baas, J. H. (1999), An empirical model for the development and equilibrium morphology of current ripples in fine sand, *Sedimentology*, *46*, 123–138.

Baas, J. H., A. P. Oost, O. K. Sztano, P. L. de Boer, and G. Postma (1993), Time as an independent variable for current ripples developing towards linguoid equilibrium morphology, *Terra Nova*, *5*, 29–35.

Bennett, S. J., and J. L. Best (1995), Mean flow and turbulence structure over fixed, two-dimensional dunes: Implications for sediment transport and bedform stability, *Sedimentology*, *42*, 491–513.

Best, J. (2005a), The fluid dynamics of river dunes: A review and some future research directions, *J. Geophys. Res.*, *110*, F04S02, doi:10.1029/2004JF000218.

Best, J. L. (2005b), The kinematics, topology and significance of dune related macroturbulence: Some observations from the laboratory and field, in *Fluvial Sedimentology VII*, edited by M. D. Blum, S. B. Marriott, and S. Leclair, *Spec. Publ. Int. Assoc. Sedimentol.*, *35*, 41–60.

Best, J., and R. Kostaschuk (2002), An experimental study of turbulent flow over a low-angle dune, *J. Geophys. Res.*, *107*(C9), 3135, doi:10.1029/2000JC000294.

Best, J., S. Bennett, J. Bridge, and M. Leeder (1997), Turbulence modulation and particle velocities over flat sand beds at low transport rates, *J. Hydraul. Eng.*, *123*, 1118–1129.

Biron, P., A. G. Roy, and J. L. Best (1995), A scheme for resampling, filtering, and subsampling unevenly spaced laser Doppler anemometer data, *Math. Geol.*, *27*, 731–748.

Bradshaw, P. (1971), *An Introduction to Turbulence and its Measurement*, Pergamon, Toronto.

Engel, P. (1981), Length of flow separation over dunes, *J. Hydraul. Div. Am. Soc. Civ. Eng.*, *107*, 1133–1143.

Kline, S. J. W., W. C. Reynolds, F. A. Schraub, and P. W. Rundstadler (1967), The structure of turbulent boundary layers, *J. Fluid Mech.*, *30*, 741–773.

Kostaschuk, R. A., and G. M. MacDonald (1988), Multitrack surveying of large bedforms, *Geo Mar. Lett.*, *8*, 57–62.

Lane, S. N., P. M. Biron, K. F. Bradbrook, J. B. Butler, J. H. Chandler, M. D. Crowell, S. J. McLelland, K. S. Richards, and A. G. Roy (1998), Three-dimensional measurement of river channel flow processes using acoustic Doppler velocimetry, *Earth Surf. Processes Landforms*, *23*, 1247–1267.

Lohrmann, A., R. Cabrera, and N. C. Kraus (1994), Acoustic-Doppler velocimeter (ADV) for laboratory use, in *Proceedings of Fundamentals and Advancements in Hydraulic Measurements and Experimentation*, pp 351–365, Am. Soc. of Civ. Eng., Buffalo, N. Y.

Lyn, D. A. (1993), Turbulence measurements in open-channel flow over bedforms, *J. Hydraul. Eng.*, *119*, 306–326.

Maddux, T. B., J. M. Nelson, and S. R. McLean (2003a), Turbulent flow over three-dimensional dunes: 1. Free surface and flow response, *J. Geophys. Res.*, *108*(F1), 6009, doi:10.1029/2003JF000017.

Maddux, T. B., S. R. McLean, and J. M. Nelson (2003b), Turbulent flow over three-dimensional dunes: 2. Fluid and bed stresses, *J. Geophys. Res.*, *108*(F1), 6010, doi:10.1029/2003JF000018.

Martin, V. (2002), Hydraulic roughness of armoured gravel beds: The role of grain protrusion, Ph.D. thesis, Univ. of B. C., Vancouver.

McLean, S. R. (1990), The stability of ripples and dunes, *Earth Sci. Rev.*, *29*, 131–144.

McLean, S. R., J. M. Nelson, and S. R. Wolfe (1994), Turbulence structure over two-dimensional bed forms: Implications for sediment transport, *J. Geophys. Res.*, *99*, 12,729–12,747.

McLean, S. R., J. M. Nelson, and S. R. Wolfe (1999), Spatially averaged flow over a wavy boundary revisited, *J. Geophys. Res.*, *104*, 15,743–15,753.

Nelson, J. M., and J. D. Smith (1986), Mechanics of flow over ripples and dunes, *J. Geophys. Res.*, *94*, 8146–8162.

Nelson, J. M., S. R. McLean, and S. R. Wolfe (1993), Mean flow and turbulence over two-dimensional bed forms, *Water Resour. Res.*, *29*, 3935–3953.

Nezu, I., and H. Nakagawa (1993), *Turbulence in Open-Channel Flows*, A. A. Balkema, Rotterdam, Netherlands.

Nezu, I., and W. Rodi (1986), Open-channel flow measurements with a laser Doppler anemometer, *J. Hydraul. Eng.*, *112*, 335–355.

Parsons, D. R., J. L. Best, O. Orfeo, R. J. Hardy, R. Kostaschuk, and S. N. Lane (2005), Morphology and flow fields of three-dimensional dunes, Rio Paraná, Argentina: Results from simultaneous multibeam echo sounding and acoustic Doppler current profiling, *J. Geophys. Res.*, *110*, F04S03, doi:10.1029/2004JF000231.

Schindler, R. J., and A. Robert (2005), Flow and turbulence structure across the ripple-dune transition: An experiment under mobile bed conditions, *Sedimentology*, *52*, 627–649, doi:10.1111/j.1365-3091.2005.00706x.

Schmeeckle, M. W., Y. Shimizu, K. Hoshi, H. Baba, and S. Ikezaki (1999), Turbulent structures and suspended sediment over two-dimensional dunes, in *River, Coastal and Estuarine Morphodynamics, Proceedings International Association for Hydraulic Research Symposium*, edited by G. Seminara and P. Blondeaux, pp. 261–270, Springer, New York.

Shimizu, Y., M. W. Schmeeckle, K. Hoshi, and K. Tateya (1999), Numerical simulation of turbulence over two-dimensional dunes, in *River, Coastal and Estuarine Morphodynamics, Proceedings International Association for Hydraulic Research Symposium*, edited by G. Seminara and P. Blondeaux, pp. 251–260, Springer, New York.

Shimizu, Y., M. W. Schmeeckle, and J. M. Nelson (2001), Direct numerical simulation of turbulence over two-dimensional dunes using CIP methods, *J. Hydrosci. Hydraul. Eng.*, *19*(2), 85–92.

Sirovich, L., and S. Karlsson (1997), Turbulent drag reduction by passive mechanisms, *Nature*, *388*, 753–755.

Smith, J. D., and S. R. McLean (1977), Spatially averaged flow over a wavy boundary, *J. Geophys. Res.*, *82*, 1735–1746.

Sontek (1997), ADV operation manual, software version 4.0, Sontek, San Diego, Calif.

Tennekes, H., and J. L. Lumley (1972), *A First Course in Turbulence*, MIT Press, Cambridge, Mass.

Venditti, J. G. (2003), The initiation and development of sand dunes in river channels, Ph.D. thesis, Univ. of B. C., Vancouver.

Venditti, J. G., and B. O. Bauer (2005), Turbulent flow over a dune: Green River, Colorado, *Earth Surf. Processes Landforms*, *30*, 289–304, doi:10.1002/esp.1142.

Venditti, J. G., and S. J. Bennett (2000), Spectral analysis of turbulent flow and suspended sediment transport over fixed dunes, *J. Geophys. Res.*, *105*, 22,035–22,047.

Venditti, J. G., M. Church, and S. J. Bennett (2005a), On the transition between 2D and 3D dunes, *Sedimentology*, *52*, 1343–1359, doi:10.1111/j.1365-3091.2005.00748.x.

Venditti, J. G., M. Church, and S. J. Bennett (2005b), Bed form initiation from a flat sand bed, *J. Geophys. Res.*, *110*, F01009, doi:10.1029/2004JF000149.

Venditti, J. G., M. Church, and S. J. Bennett (2005c), Morphodynamics of small-scale superimposed sand waves over migrating dune bed forms, *Water Resour. Res.*, *41*, W10423, doi:10.1029/2004WR003461.

Wiberg, P. L., and J. M. Nelson (1992), Unidirectional flow over a asymmetric and symmetric ripples, *J. Geophys. Res.*, *97*, 12,745–12,761.

Williams, G. P. (1970), Flume width and water depth effects in sediment transport experiments, *U.S. Geol. Surv. Prof. Pap.*, *37*, 562-H.

Zedler, E. A., and R. L. Street (2001), Large-eddy simulation of sediment transport currents over ripples, *J. Hydraul. Eng.*, *127*, 444–452.

J. G. Venditti, Department of Geography, Simon Fraser University, 888 University Drive, Burnaby, BC, Canada V5A 1S6. (jgvenditti@yahoo.ca)